Article

Cell Stem Cell

Tbx6 Induces Nascent Mesoderm from Pluripotent Stem Cells and Temporally Controls Cardiac versus Somite Lineage Diversification

Graphical Abstract

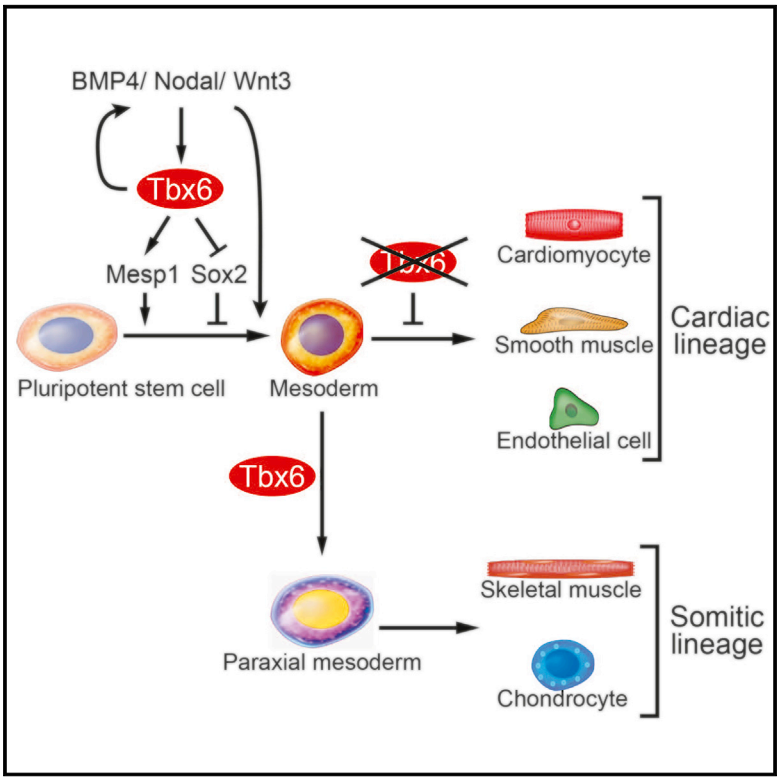

Authors

Taketaro Sadahiro, Mari Isomi, Naoto Muraoka, ..., Hirofumi Nishizono, Keiichi Fukuda, Masaki Ieda

Correspondence

mieda@md.tsukuba.ac.jp

In Brief

Sadahiro et al. show that Tbx6 is critical for mesoderm induction and subsequent lineage diversification from pluripotent stem cells (PSCs). Transient Tbx6 expression induced nascent mesoderm and cardiovascular lineages from mouse and human PSCs, whereas prolonged Tbx6 expression suppressed cardiac differentiation and induced somite lineages, including skeletal muscle and chondrocytes.

Highlights

- Direct reprogramming-based screening identifies Tbx6 as a mesoderm-inducing factor
- Tbx6 is critical for PSC differentiation into mesoderm and cardiovascular lineages
- Tbx6 directly upregulates Mesp1, inhibits Sox2, and activates BMP/Nodal/Wnt signaling
- Prolonged Tbx6 expression inhibits cardiac specification and induces somite lineages

Data Resources

GSE89820

Sadahiro et al., 2018, Cell Stem Cell *23*, 382–395
September 6, 2018
https://doi.org/10.1016/j.stem.2018.07.001

CellPress

CellPress

Cell Stem Cell
Article

Tbx6 Induces Nascent Mesoderm from Pluripotent Stem Cells and Temporally Controls Cardiac versus Somite Lineage Diversification

Taketaro Sadahiro,[1] Mari Isomi,[1] Naoto Muraoka,[1,2] Hidenori Kojima,[1] Sho Haginiwa,[1] Shota Kurotsu,[1] Fumiya Tamura,[1] Hidenori Tani,[1] Shugo Tohyama,[1] Jun Fujita,[1] Hiroyuki Miyoshi,[2] Yoshifumi Kawamura,[3] Naoki Goshima,[4] Yuka W. Iwasaki,[5] Kensaku Murano,[5] Kuniaki Saito,[5,6,7] Mayumi Oda,[8] Peter Andersen,[9] Chulan Kwon,[9] Hideki Uosaki,[9,10] Hirofumi Nishizono,[11] Keiichi Fukuda,[1] and Masaki Ieda[12,13,*]

[1]Department of Cardiology, Keio University School of Medicine, 35 Shinanomachi, Shinjuku-ku, Tokyo 160-8582, Japan
[2]Department of Physiology, Keio University School of Medicine, 35 Shinanomachi, Shinjuku-ku, Tokyo 160-8582, Japan
[3]Japan Biological Informatics Consortium (JBiC), Koto-ku, Tokyo 135-8073, Japan
[4]Molecular Profiling Research Center for Drug Discovery, National Institute of Advanced Industrial Science and Technology, Koto-ku, Tokyo 135-0064, Japan
[5]Department of Molecular Biology, Keio University School of Medicine, 35 Shinanomachi, Shinjuku-ku, Tokyo 160-8582, Japan
[6]Invertebrate Genetics Laboratory, National Institute of Genetics, Research Organization of Information and Systems (ROIS), Mishima, Shizuoka 411-8540, Japan
[7]Department of Genetics, The Graduate University for Advanced Studies (SOKENDAI), Hayama, Kanagawa 240-0193, Japan
[8]Department of Systems Medicine, Keio University School of Medicine, 35 Shinanomachi, Shinjuku-ku, Tokyo 160-8582, Japan
[9]Division of Cardiology, Institute for Cell Engineering, Johns Hopkins University School of Medicine, Baltimore, MD 21205, USA
[10]Division of Regenerative Medicine, Center for Molecular Medicine, Jichi Medical University, Shimotsuke, Tochigi 329-0498, Japan
[11]Life Science Research Center, University of Toyama, Sugitani, Toyama 930-0194, Japan
[12]Department of Cardiology, Faculty of Medicine, University of Tsukuba, 1-1-1 Tennoudai, Tsukuba City, Ibaraki 305-8575, Japan
[13]Lead Contact
*Correspondence: mieda@md.tsukuba.ac.jp
https://doi.org/10.1016/j.stem.2018.07.001

SUMMARY

The mesoderm arises from pluripotent epiblasts and differentiates into multiple lineages; however, the underlying molecular mechanisms are unclear. Tbx6 is enriched in the paraxial mesoderm and is implicated in somite formation, but its function in other mesoderms remains elusive. Here, using direct reprogramming-based screening, single-cell RNA-seq in mouse embryos, and directed cardiac differentiation in pluripotent stem cells (PSCs), we demonstrated that Tbx6 induces nascent mesoderm from PSCs and determines cardiovascular and somite lineage specification via its temporal expression. Tbx6 knockout in mouse PSCs using CRISPR/Cas9 technology inhibited mesoderm and cardiovascular differentiation, whereas transient Tbx6 expression induced mesoderm and cardiovascular specification from mouse and human PSCs via direct upregulation of Mesp1, repression of Sox2, and activation of BMP/Nodal/Wnt signaling. Notably, prolonged Tbx6 expression suppressed cardiac differentiation and induced somite lineages, including skeletal muscle and chondrocytes. Thus, Tbx6 is critical for mesoderm induction and subsequent lineage diversification.

INTRODUCTION

In mammals, all organs are derived from three primary germ layers, mesoderm, endoderm, and ectoderm. Nascent mesoderm is induced as epiblast cells ingress through the primitive streak (PS), and distinct mesoderm populations are specified according to the timing and order of cell migration. The heart is derived from lateral/cardiac mesoderm and is the first functional organ to be formed in embryos. The lateral/cardiac mesoderm arises from the mid PS and moves anteriorly to be specified to cardiac progenitor cells (CPCs) that differentiate into cardiomyocytes (CMs), smooth muscle cells (SMCs), and endothelial cells (ECs) (Paige et al., 2012; Wamstad et al., 2012). The paraxial/presomitic mesoderm subsequently arises from the anterior PS and differentiates into the somite, in which the axial skeleton, skeletal muscle, and dermis are formed (Loh et al., 2016). Understanding the regulation of mesoderm development is critical for generating each of these cell types and elucidating the mechanisms of congenital diseases.

Pluripotent stem cell (PSC)-based differentiation recapitulates the developmental process in embryos and represents a valuable platform to study the mechanisms of cell-fate specification. Previous studies have revealed that temporal activation and inhibition of bone morphogenic protein (BMP), Nodal/Activin, and Wnt signaling induced nascent mesoderm and multiple mesodermal derivatives from PSCs. Wnt activation induced nascent mesoderm from PSCs, but, once

mesoderm was induced, inhibition of Wnt signaling was necessary for cardiac specification and prolonged Wnt/β-catenin activation inhibited cardiac differentiation and instead, induced other lineages, including paraxial mesoderm (Burridge et al., 2014; Kattman et al., 2011; Lian et al., 2012; Loh et al., 2016). Despite recent success in directed differentiation from PSCs with a series of small molecules and cytokines, the molecular mechanisms for mesoderm induction and lineage diversification remain elusive, since mesoderm development is a dynamic process and the sample sizes were too small for conventional genome-wide analyses. Recent single-cell RNA sequencing (RNA-seq) profiling revealed the landscape for temporal and spatial changes of gene expression in early/nascent mesoderm and subsequent lineage specification *in vivo* and *in vitro* (Loh et al., 2016; Scialdone et al., 2016). However, a single transcription factor sufficient to induce nascent mesoderm without exogenous factors is unknown, and regulatory mechanisms for mesodermal lineage diversification remain poorly understood.

Direct reprogramming may identify new key regulators for lineage commitment via screening of candidate genes. Overexpression of reprogramming factors in fibroblasts may induce new programs of desired cell types within a week, which might be simpler and faster than generating multiple PSC-lines expressing a series of candidate genes. We previously demonstrated that a combination of cardiac-enriched transcription factors, *Gata4*, *Mef2c*, and *Tbx5*, directly reprogrammed mouse fibroblasts into functional CMs by screening 14 factors (Ieda et al., 2010; Sadahiro et al., 2015); however, genes that induce nascent mesoderm have not been identified.

Tbx6 is a T-box transcription factor enriched in paraxial/presomitic mesoderm. Tbx6 has been implicated in somite formation, with Tbx6 mutant mice generating two ectopic neural tubes at the expense of somite formation, but its expression and function in early/nascent mesoderm and other mesodermal derivatives, including cardiovascular lineages, remain largely unknown (Chapman and Papaioannou, 1998; Takemoto et al., 2011; Wardle and Papaioannou, 2008). Here, we attempted to identify a defined factor that could induce nascent mesoderm from mouse and human PSCs in the absence of exogenous factors and determine its function in mesodermal lineage diversification.

RESULTS

Direct Reprogramming-Based Screening Identified Tbx6 as a Mesoderm-Inducing Factor in Mouse Fibroblasts

To identify new key regulators for nascent mesoderm, we adopted direct reprogramming-based screening. We selected 58 candidate transcription factors expressed in mesodermal lineages and important for development, including *Eomes*, *Ets2*, *Lef1*, *Tcf3*, *Smads*, *T*, *Tbx3*, and *Tbx6* (Islas et al., 2012; Weidgang et al., 2013). These 58 genes were cloned individually into pMX retroviral vectors for efficient and continuous gene expression in fibroblasts (Ieda et al., 2010). We used mouse embryonic fibroblasts (MEFs) that were not contaminated with nascent mesoderm and cardiovascular cells. We transduced each retroviral vector into MEFs and analyzed the induction of *Mesp1*, a marker for early/nascent mesoderm, after 1 week of transduction. Intriguingly, among 58 factors, only Tbx6 strongly induced *Mesp1* mRNA expression (Figure 1A). Moreover, the addition of Eomes or T, two other mesoderm-enriched T-box transcription factors, to Tbx6 did not further upregulate *Mesp1* expression in MEFs (Figure 1B). We next utilized MEFs from $Mesp1^{cre/+}$ (Mesp1-Cre)/GFP-flox mice, in which the Mesp1-expressing mesoderm and its progeny can be traced by GFP expression (Saga et al., 1999). We found that Tbx6-transduced MEFs expressed GFP, which was not detected in the uninfected MEFs. The Mesp1-Cre/GFP^+ cells formed multiple colonies but did not proliferate indefinitely, similar to those *in vivo* (Figure 1C). We also analyzed the expression of T/Brachyury, another marker of nascent mesoderm. Immunostaining demonstrated that T protein was also expressed in the Tbx6-transduced cell nuclei after 4 weeks (Figure 1D). Next, we analyzed two surface markers for mesoderm, Flk1 and PDGFRα (Kattman et al., 2011; Liu et al., 2016). Fluorescence-activated cell sorting (FACS) analyses revealed that Flk1 and PDGFRα-double positive cells, markers for lateral/cardiac mesoderm population, were detected in ~5% of the Tbx6-transduced fibroblasts after 4 weeks (Figure 1E). We next analyzed the gene expression profile related to the mesoderm (*Mesp1*, *T*, *Flk1*), CPCs (*Isl1*, *Nkx2.5*, *Gata4*), CMs (*Tnnt2*, *Myh6*), SMCs (*Myh11*), ECs (*Pecam1*), and skeletal muscles (*Pax3*, *Pax7*, *Myod1*, *Myf5*), in Tbx6-transduced MEFs over time. qRT-PCR analyses revealed that mesoderm-related genes were upregulated and remained high even after 4 weeks, whereas the expression of CPC, CM, SMC, EC, and skeletal muscle genes was not activated, except for *Isl1*, a marker for early CPCs (Figure 1F). These results suggest that continuous Tbx6 expression induced and maintained an early/nascent mesoderm program in mouse fibroblasts.

Single-Cell RNA-Seq Revealed that $Tbx6^+$ Nascent Mesoderm Expresses Genes Related to Cardiovascular Mesoderm and Early CPCs in Mouse Embryos

Tbx6 is essential for the development of somites. Tbx6 expression is first detected in the PS at embryonic day (E) 7.0 during gastrulation and later restricted in the paraxial/presomitic mesoderm and tail bud from E8.5 to E12.5 in mouse embryos (Chapman et al., 1996). However, the precise nature of the early mesoderm population expressing Tbx6 remains unclear, because the cell numbers are too small for conventional genome-wide analyses. To investigate the spatiotemporal transcriptional profiles associated with Tbx6 expression in mouse embryos, we analyzed the publicly available single-cell RNA-seq data for the 682 single cells of the FACS $Flk1^+$ mesoderm and $CD41^+$ cells in mouse embryos at E7.0–7.75 (Scialdone et al., 2016). The t-distributed stochastic neighbor embedding (t-SNE) projection and expression of key marker genes divided the single cells into seven major groups: nascent mesoderm, posterior mesoderm, endothelium, blood progenitors, embryonic blood, allantois, and pharyngeal mesoderm (Figure S1A). Among them, Tbx6

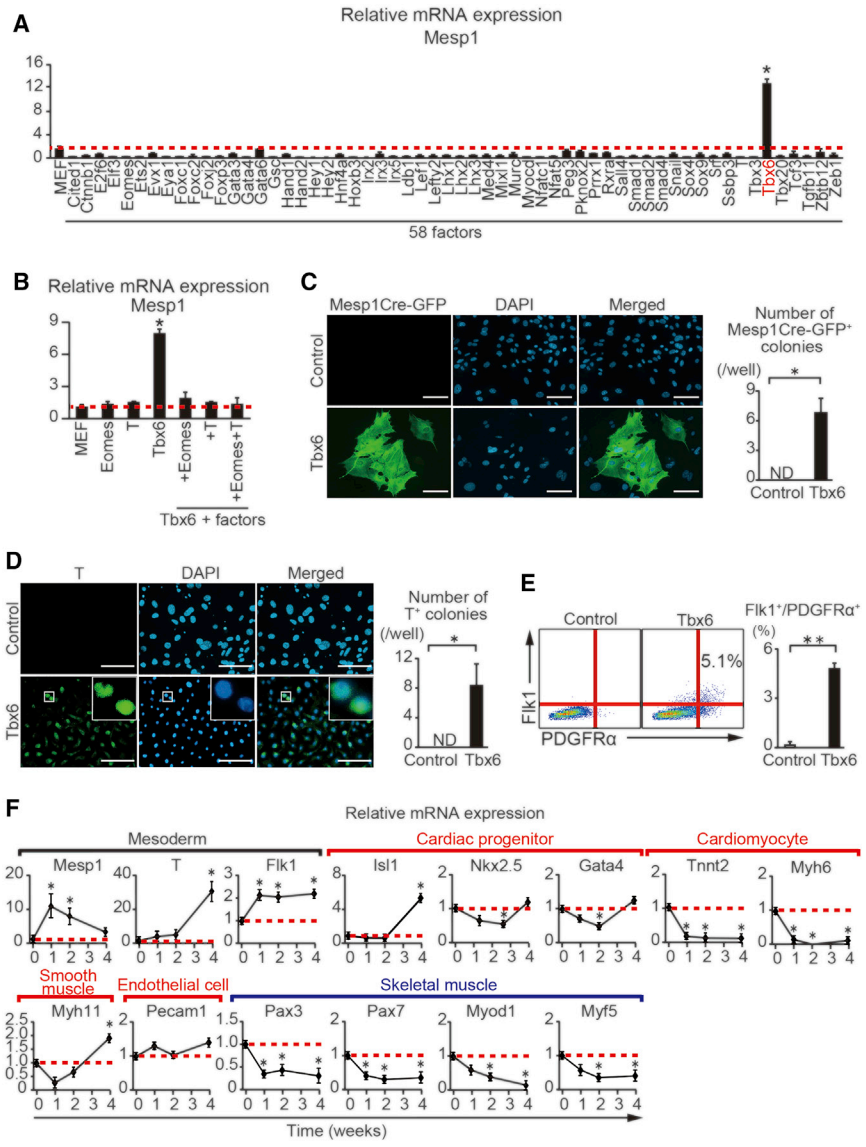

Figure 1. Tbx6 Induced and Maintained a Mesoderm Program in Mouse Fibroblasts

(A and B) qRT-PCR for *Mesp1* expression after transduction of individual (A) or combinatorial (B) factors after 1 week (n = 3, independent experiments). Data were normalized to the values in MEFs.

(C) Immunocytochemistry for Mesp1Cre-GFP and DAPI with quantification of the numbers of Mesp1Cre-GFP$^+$ colonies (n = 3, independent experiments). Tbx6 induced Mesp1Cre-GFP expression after 2 weeks of transduction.

(D) Immunocytochemistry and quantification of the numbers of T$^+$ colonies (n = 3, independent experiments). Immunocytochemistry demonstrated that T protein was expressed in Tbx6-transduced mouse embryonic fibroblast nuclei after 4 weeks.

(E) FACS analyses showed that Tbx6-transduced cells expressed cell-surface markers Flk1 and PDGFRα (n = 3, independent experiments).

(F) Time course of mRNA expression in MEFs transduced with Tbx6, as determined by qRT-PCR. Gene expression for mesoderm (*Mesp1*, *T*, *Flk1*), CPCs (*Isl1*, *Nkx2.5*, *Gata4*), CMs (*Tnnt2*, *Myh6*), SMCs (*Myh11*), ECs (*Pecam1*), and skeletal muscle (*Pax3*, *Pax7*, *Myod1*, *Myf5*) genes were determined. Tbx6-transduced cells expressed mesoderm genes, but not those associated with cardiovascular differentiation and skeletal muscle genes. Data were normalized to the values on day 0.

All data are presented as mean ± SD. $^{**}p < 0.01$; $^{*}p < 0.05$ versus MEFs (A and B), control (C–E), or day 0 (F). Scale bars represent 100 μm.

was specifically expressed in a large population of the E7.0 nascent mesoderm group (Figure 2A). Tbx6 expression was correlated with other nascent mesoderm-associated genes, including *T*, *Mixl1*, and *Mesp1*, with *Mesp1* more broadly expressed in this and other populations, such as the posterior and pharyngeal mesoderm, consistent with its known expression profile (Chan et al., 2013; Saga et al., 1999). Intriguingly, Tbx6$^+$ nascent mesoderm was correlated with the expression of lateral/cardiac mesoderm genes (*Flk1*, *Pdgfrα*) and early CPC genes (*Isl1*, *Gata4*) rather than paraxial/presomitic mesoderm genes (*Msgn1*, *Meox1*) at this early stage. Tbx6$^+$ mesoderm cells neither expressed late CPC/CM genes (*Nkx2.5*, *Tbx5*), skeletal muscle genes (*Pax3*, *Pax7*, *Myod1*, *Myf5*), nor a definitive endoderm gene (*Foxa2*) (Figures 2B and S1B). These results suggest that Tbx6 is expressed in the nascent mesoderm population related to cardiovascular mesoderm/progenitors rather than paraxial/presomitic mesoderm in early mouse embryos.

Tbx6 Is Critical for Mouse ESC Differentiation into Mesoderm and Cardiovascular Lineages

Next, to investigate the kinetics and roles of Tbx6 in cardiogenesis in detail, we used a mouse ESC-based directed cardiac differentiation system, in which the mesoderm, CPCs, and CMs were sequentially induced (Kattman et al., 2011). T$^{GFP/+}$ mouse ESCs (T-GFP ESCs) were used to mark the nascent mesoderm population (Kattman et al., 2006). Embryoid bodies (EBs) were generated and cultured for 2 days in the absence of exogenous factors (days 0–2), subsequently treated with Activin A, BMP4, and vascular endothelial growth factor (VEGF) (ABV) for 2 days to induce mesoderm under serum-free conditions (days 2–4), and then dissociated to a monolayer culture to differentiate into CPCs and CMs (days 4–14) (Figure 3A). This directed cardiac differentiation protocol efficiently specified the T-GFP ESCs into mesoderm and CMs (Figures 3B–3D and S2A). qRT-PCR revealed that Tbx6 mRNA expression was rapidly induced at the mesoderm stage, peaking on day 4, and was sharply downregulated thereafter. This was similar to the kinetics of other nascent mesodermal genes, such as *Eomes*, *T*, and *Mesp1*, but not to those of paraxial mesoderm genes (*Msgn1*, *Meox1*, *Tcf15*) or skeletal muscle genes (*Pax3*, *Pax7*, *Myog*) (Figures 3C and S2B). The CPC and CM genes

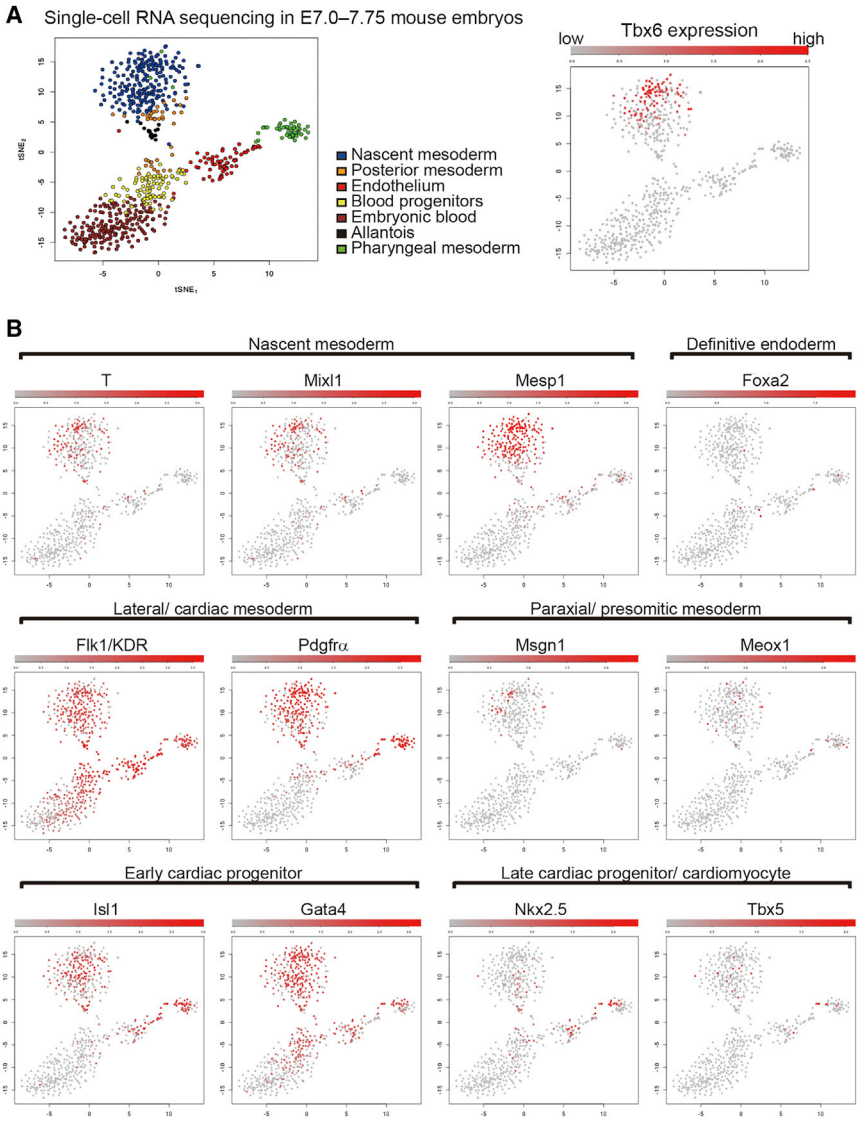

Figure 2. Single-Cell RNA-Seq Revealed the Transcriptional Profile in Tbx6$^+$ Nascent Mesoderm in Mouse Embryos

(A) Single-cell RNA-seq in E7.0–7.75 mouse embryos. FACS was used to sort single cells as Flk1$^+$ mesoderm cells and CD41$^+$ cells. t-SNE for 682 single cells was colored by assigned groups with varying contributions from different embryonic stages. The expression of key marker genes assigned identities to each group (left). Points were colored red depending on the expression of Tbx6 (right).

(B) t-SNE for 682 cells from E7.0–7.75 mouse embryos. Each point was colored according to the expression of each gene. Single cells from mouse embryos acquired at E7.0 (138 cells, 3 embryos), E7.5 (259 cells, 12 embryos), and E7.75 (307 cells, 11 embryos) were analyzed.

See also Figure S1.

Nkx2.5, *Tnnt2*, and *Myh6* were induced from day 6, and *Isl1* expression started on day 4 and peaked on day 6. Thus, the expression kinetics of Tbx6 *in vitro* is consistent with the single-cell RNA-seq results in early mouse embryos. Next, to determine whether Tbx6 is expressed in the mesoderm but not in other populations in day 4 EBs, we used FACS to sort T-GFP$^+$ and T-GFP$^-$ cells for the analysis of gene expression (Figures 3B and 3D). Tbx6 expression was significantly enriched in the T-GFP$^+$ population, corresponding to *T* and *Mesp1* expression, whereas *Sox2* was expressed in T-GFP$^-$ cells, suggesting that Tbx6 was expressed in the mesoderm (Figure 3D).

It has been reported that neuromesodermal progenitors (NMPs; T and Sox2 double-positive cells) play a role in embryonic development and differentiate into both neural and mesodermal lineages (Gouti et al., 2014). We next tested whether NMPs were induced in this directed cardiac differentiation protocol. qRT-PCR and immunocytochemistry revealed that T$^+$/Sox2$^+$ NMPs were not induced prior to mesoderm, CPC, and CM differentiation (Figures S2B and S2C).

Next, to investigate whether Tbx6 is critical for mesoderm specification and cardiovascular differentiation in mouse ESCs, we generated Tbx6 knockout (KO) ESCs using the CRISPR/Cas9 system (Figure 3E). To generate Tbx6 KO ESCs, guide RNA was targeted to the first exon of Tbx6, an RFP and blasticidin cassette was knocked into one allele, and CRISPR/Cas9-mediated DNA deletion leading to frameshift mutation was introduced into another allele in E14 wild-type (WT) ESCs. DNA sequencing and PCR analyses confirmed the integrity of three clonal Tbx6 KO ESC lines (clones #1–3, Figures S3A–S3C). We first differentiated clone #1 Tbx6 KO ESCs into cardiovascular lineages with directed differentiation and compared these to the parental WT ESCs (Figure 3F). qRT-PCR demonstrated that *T*, *Mesp1*, and *Eomes* mRNA expression was significantly downregulated in the Tbx6 KO EBs on day 4 (Figure 3G). Consequently, induction of Flk1$^+$/PDGFRα$^+$ presumptive lateral/cardiac mesoderm was significantly suppressed in the Tbx6 KO EBs compared to that in WT EBs (Figures 3H and 3J). Moreover, cardiac differentiation, determined by the presence of cTnT$^+$ cells, was significantly reduced in clone #1 Tbx6 KO ESCs to one-third of that in WT ESCs on day 14 (Figures 3I and 3J). qRT-PCR analyses also revealed that multiple cardiovascular genes, including *Actn2*, *Tnnt2*, *Nkx2.5*, *Myh11*, and *Pecam1*, were suppressed in the Tbx6 KO ESCs (Figure S3D). Next, to determine the reproducibility of multiple Tbx6 KO ESC lines in mesoderm and CM induction, we analyzed two other Tbx6 KO ESC lines (clone #2 and #3). FACS analyses revealed that induction of Flk1$^+$/PDGFRα$^+$ and cTnT$^+$ cells was significantly suppressed in the clone #2 and #3 Tbx6 KO ESCs (Figures 3J, S3E, and S3F). These results suggest that Tbx6, transiently expressed in the nascent mesoderm,

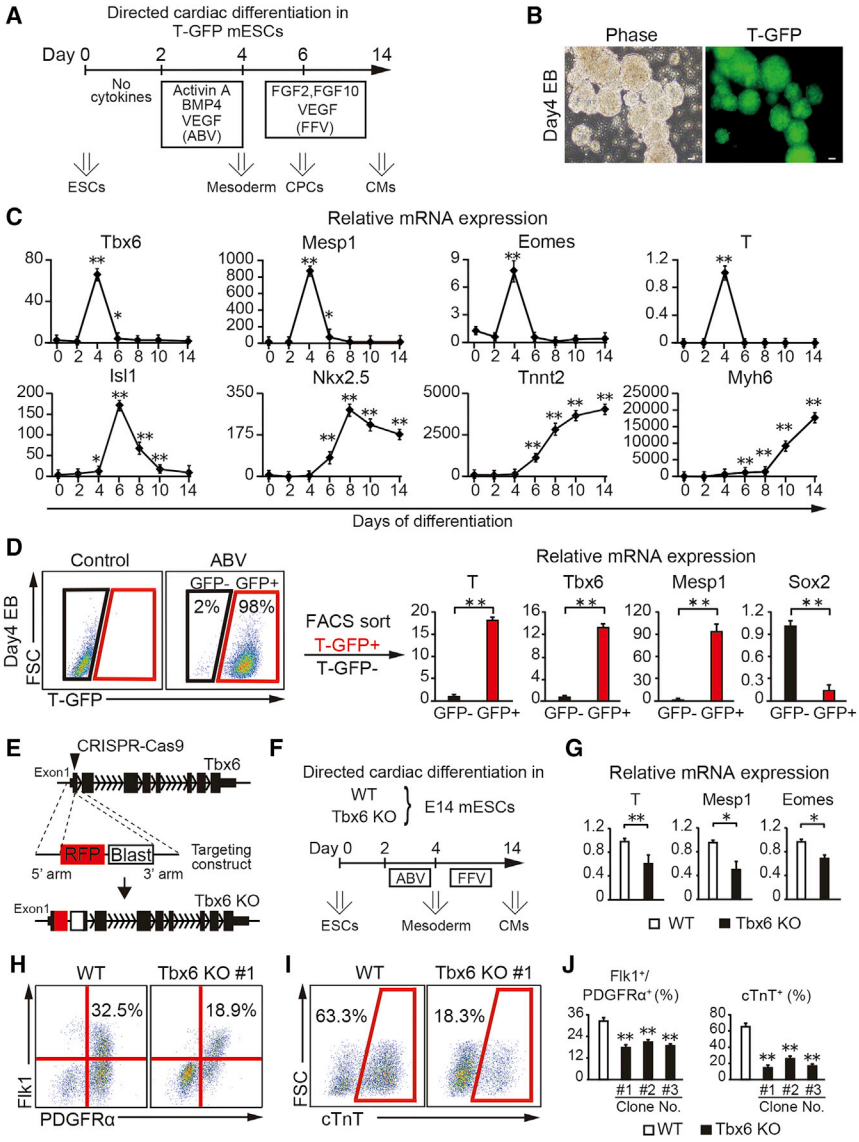

Figure 3. Tbx6 Was Transiently Expressed in Mesoderm Prior to CPC and CM Differentiation in Mouse ESCs

(A) Schematic representation of the directed cardiac differentiation protocol in T-GFP mouse ESCs.

(B) GFP was induced in the T-GFP embryoid bodies (EBs) after 4 days of differentiation.

(C) Time course of mRNA expression during ESC differentiation determined by qRT-PCR. Data were normalized to the values on day 0.

(D) Relative mRNA expression of mesoderm genes (*Tbx6*, *T*, *Mesp1*) and *Sox2* in the FACS T-GFP$^+$ cells and T-GFP$^-$ cells after 4 days of differentiation (n = 3, independent experiments). Data were normalized to the values in T-GFP$^-$ cells.

(E) Generation of the Tbx6 KO mouse ESCs using the CRISPR/Cas9 system. See also Figure S1 in detail.

(F) WT or Tbx6 KO mouse ESCs were differentiated into mesoderm and CMs using a directed cardiac differentiation protocol.

(G) Relative mRNA expression was determined by qRT-PCR in day 4 EBs (n = 3, independent experiments). Data were normalized to the values obtained in WT ESCs.

(H–J) FACS analysis for Flk1/PDGFRα and cTnT expression in the WT or clone #1 Tbx6 KO ESCs after 4 (H) or 14 days (I) of differentiation. Quantitative data are from WT and Tbx6 KO ESCs (clones #1–3) are shown in (J) (n = 3, independent experiments).

All data are presented as the mean ± SD. $^{**}p < 0.01$; $^{*}p < 0.05$ versus day 0 (C), T-GFP$^-$ cells (D), or WT ESCs (G and J). Scale bars represent 100 μm. See also Figures S2 and S3.

is critical for mouse ESC differentiation into mesoderm and subsequent cardiovascular lineages.

Transient Tbx6 Expression Induces Mesoderm and Cardiovascular Lineages in Mouse ESCs

Next, to investigate the effect of Tbx6 on mesoderm induction and cardiovascular differentiation in ESCs, we generated clonal T-GFP mouse ESC lines, in which the expression of FLAG-tagged mouse Tbx6 could be induced by doxycycline (Dox) administration and mesoderm induction could be monitored by GFP expression (iTbx6 T-GFP mESCs) (Figures 4A and 4B). Humanized Kusabira-Orange fluorescence (hKO) was used for homogeneous and clonal expansion of the mouse ESCs, and Tbx6 expression was confirmed following Dox administration (Figures 4B, 4C, and S4A). As a control experiment, we first confirmed that iTbx6 T-GFP mESCs efficiently differentiated into mesoderm and CMs by the addition of multiple cytokines (Activin A, BMP4, and VEGF: ABV) with similar efficiency to those in parental mouse ESCs, suggesting that they possessed intact differentiation potential (ABV, Figures 4D–4I and S4B). In contrast, in the absence of cytokines (ABV) and Dox administration (No Dox), the mouse ESCs never differentiated into T-GFP$^+$ or Flk1$^+$/PDGFRα$^+$ mesoderm and CMs (No Dox, Figures 4D–4I and S4B). Notably, Dox administration alone (Dox on) induced T-GFP$^+$ and Flk1$^+$/PDGFRα$^+$ mesoderm in the iTbx6 T-GFP mESCs in a time-dependent manner. The efficiency of mesoderm induction by Dox administration from days 0–3 was comparable to those with the directed cardiac differentiation using ABV (Dox on D0–3, Figures 4D–4G and S4B). Induction of Tbx6 on days 0–2 or 2–3 showed minimal effects, suggesting that the expression of Tbx6 for the first 3 days is critical for efficient mesoderm and cardiac induction (Figures 4D–4J and S4C). To determine the dose dependency and reproducibility of mesoderm induction by Tbx6, we next analyzed nine independent clonal iTbx6 T-GFP mESC lines, in which Tbx6 was differentially induced with Dox (Figure S4D). The mouse ESC lines expressing high Tbx6 levels (clones #7, 8, 9) showed the highest and comparable T-GFP induction, whereas cells expressing low (clones #1–3) or intermediate (clones #4–6) Tbx6 levels demonstrated lower induction of T-GFP (Figures S4D–S4F). These results suggested that transient Tbx6 expression was sufficient for the induction of mesoderm from mouse ESCs without the need for exogenous factors.

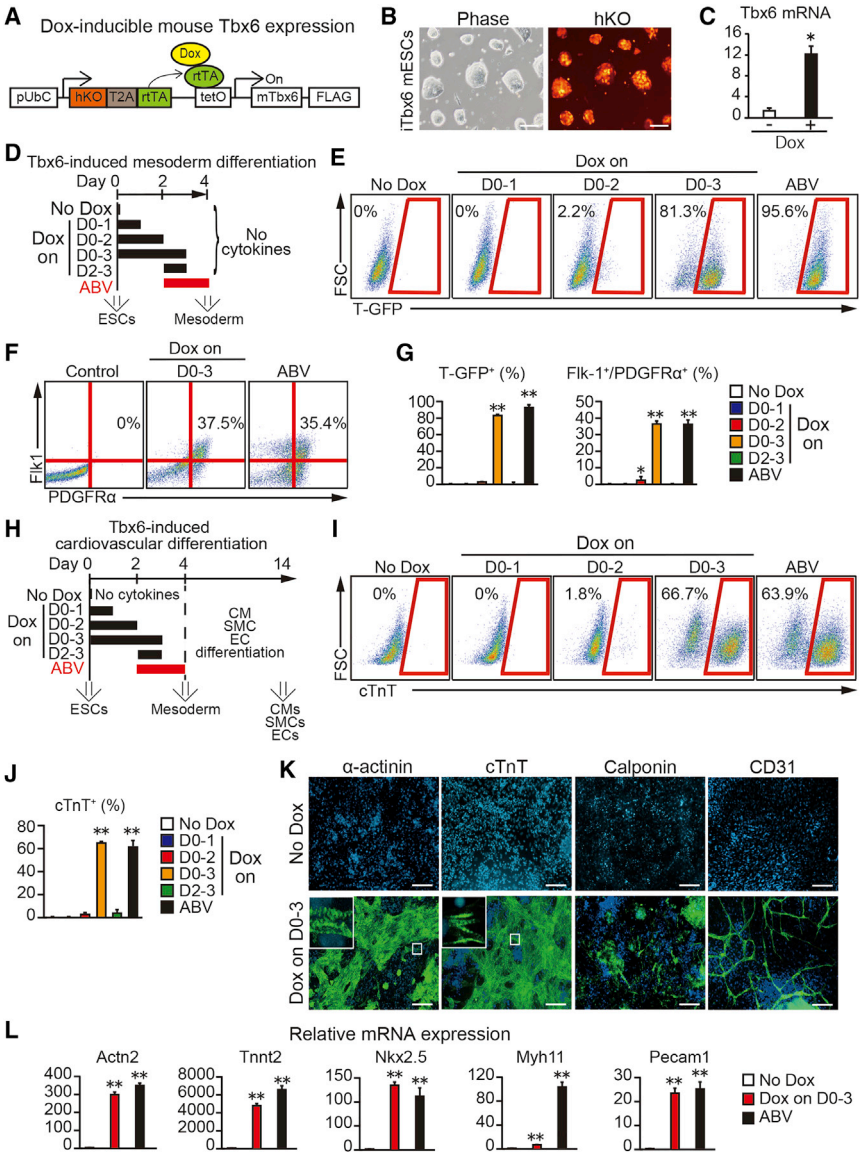

Figure 4. Transient Tbx6 Expression Induced Mesoderm and Cardiovascular Lineages in Mouse ESCs

(A) Schematic representation of the lentiviral construct for Dox-inducible Tbx6 expression.

(B) Clonal expansion of the iTbx6 T-GFP mouse ESCs was confirmed by hKO expression.

(C) The mRNA expression of *Tbx6* in iTbx6 T-GFP mESCs with or without Dox administration was determined by qRT-PCR (n = 3, independent experiments). Data were normalized to the values in No Dox.

(D) Scheme depicting the protocol used to evaluate the effects of Tbx6 expression on mesoderm induction. ABV indicates Activin A, BMP4, and VEGF.

(E–G) FACS profiles for the expression of mesoderm markers in EBs on day 4 (E and F). Quantitative data are shown in (G). See also Figure S4C.

(H) The protocol used to evaluate the effects of the duration of Tbx6 expression on cardiac differentiation.

(I and J) FACS analyses for the expression of cTnT on day 14 (I). Quantitative data are shown in (J). See also Figure S4C.

(K) iTbx6 T-GFP mESCs were differentiated into CMs, SMCs, and ECs with Dox administration for 3 days. Representative images are shown.

(L) The mRNA expression for CM, SMC, and EC genes in iTbx6 T-GFP mESCs with (red, Dox on D0–3) or without Dox (white, No Dox) in the absence of cytokines (n = 3, independent experiments). ABV (black) is cytokine-based cardiac differentiation. Data were normalized to the values in No Dox.

All data are presented as the mean ± SD. $^{**}p < 0.01$; $^{*}p < 0.05$ versus No Dox. Scale bars represent 100 μm. See also Figure S4.

We next analyzed whether Tbx6-induced mesoderm could differentiate into cardiovascular lineages. The mesoderm generated by Dox administration from days 0–3 induced ~60% of cTnT$^+$ cells after 14 days, which was comparable to that with the cytokine-based cardiac differentiation; Tbx6-induced CMs beat robustly and synchronously in culture (Dox on D0–3, Figures 4H–4J, Video S1). We also found that prolonged Tbx6 expression (longer than 3 days) suppressed cardiac differentiation (Figures 6B and 6C). Immunostaining demonstrated that Tbx6-induced mesoderm differentiated into all three cardiovascular lineages (Dox on D0–3), including CMs, SMCs, and ECs, whereas no cardiovascular cells were generated without Dox addition (No Dox, Figures 4K and S4G). qRT-PCR also revealed that the expression of cardiovascular genes was significantly induced with Dox addition (Figure 4L). Thus, transient Tbx6 expression induced mesoderm and subsequent cardiovascular differentiation in mouse ESCs.

Tbx6 Activates Mesoderm and Endoderm Programs and Represses Neuroectoderm Genes in Mouse ESCs

Next, to investigate the mechanisms responsible for Tbx6-mediated mesoderm induction in mouse ESCs, we performed microarray analyses and analyzed differentially expressed genes in iTbx6 T-GFP mESCs on days 2 and 4 with or without Dox administration (Figure 5A). Hierarchical clustering and gene ontology (GO) analyses revealed that the genes upregulated on day 2 were enriched for GO terms associated with the BMP signaling pathway, heart development, and angiogenesis, whereas downregulated genes were enriched for GO terms related to neural development (Figures 5A and 5B). Upregulated genes on day 4 were related to the transforming growth factor β (TGF-β) and BMP signaling pathways, PS and endoderm formation, and blood vessel and heart development, while downregulated genes were associated with neural/brain development (Figures 5A and 5C). Scatterplot analyses demonstrated that mesoderm- and endoderm-enriched genes were significantly upregulated with Dox administration (Figure S5A). Microarray and qRT-PCR analyses revealed that mesoderm and endoderm genes related to different functions, such as transcription factors (*Eomes*, *T*, *Mesp1*, *Isl1*, *Gsc*, *Sox17*), signaling molecules (*Bmp4*,

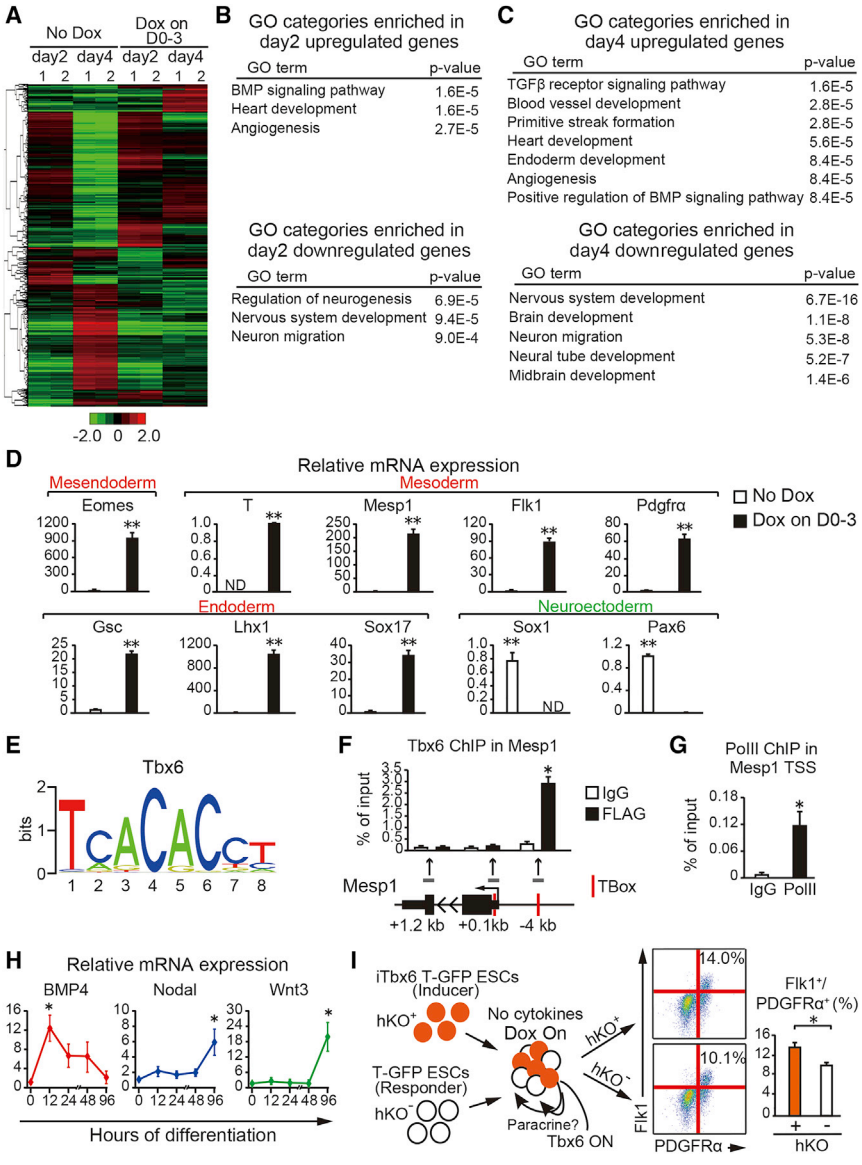

Figure 5. Tbx6 Expression Promoted Mesoderm and Endoderm Programs and Inhibited Neuroectoderm Genes in Mouse ESCs

(A) Hierarchical clustering analysis of iTbx6 T-GFP EBs with or without Dox on days 2 and 4 (n = 2). Dox was added for the first 3 days.

(B and C) GO term analyses for the upregulated and downregulated genes in iTbx6 T-GFP EBs on day 2 (B) or 4 (C) of Dox addition.

(D) Relative mRNA expression on day 4 in iTbx6 T-GFP EBs with or without Dox addition was determined by qRT-PCR (n = 3, independent experiments). Data were normalized to the values of No Dox.

(E) Consensus T-box binding site sequences generated by MEME (http://meme-suite.org/).

(F) ChIP-qPCR analyses in iTbx6 T-GFP EBs with Dox addition on day 4 using antibodies specific for FLAG (Tbx6) or IgG (control) (n = 3). Illustration of the genomic region surrounding *Mesp1*. Translated regions are depicted in thick black boxes, untranslated exons are shown in thin black boxes, and introns are shown by black lines. Conserved T-box binding sites are indicated as red lines, and the relative positions of PCR fragments for ChIP-qPCR are represented by black lines.

(G) ChIP-qPCR analysis of iTbx6 T-GFP EBs treated with Dox on day 4 using antibodies specific for RNA polymerase II (PolII) or IgG (control) (n = 3). The primers were generated near the transcriptional start site (TSS) of *Mesp1*.

(H) Time course of mRNA expression for *Bmp4*, *Nodal*, and *Wnt3* during the differentiation of ESCs after 12, 24, 48, and 96 hr of Dox treatment, determined by qRT-PCR. *Bmp4* was rapidly and strongly upregulated after only 12 hr of Dox administration.

(I) Schematic representation of chimeric EB experiments. The iTbx6 T-GFP ESCs (inducer) and T-GFP ESCs (responder) were mixed and cultured for 4 days with Dox addition from days 0–3 in the absence of cytokines before FACS. FACS analyses for Flk1 and PDGFRα expression in day 4 EBs are shown (right).

All data are presented as mean ± SD. $^{**}p < 0.01$; $^{*}p < 0.05$ versus No Dox (D), IgG (F and G), 0 hr (H), or responder (I). See also Figure S5.

Nodal, *Wnt3*), and cell-surface markers (*Flk1*, *Pdgfra*), were greatly upregulated with Dox addition, whereas neuroectoderm transcription factors (*Pax6* and *Sox1*) were significantly downregulated by Dox addition (Figures 5D and S5B). Thus, Tbx6 expression activated mesoderm and endoderm programs and concomitantly suppressed neuroectoderm gene expression in mouse ESCs to induce a mesodermal program.

Tbx6 Directly Upregulates Mesp1, Inhibits Sox2, and Activates BMP/Nodal/Wnt Paracrine Signaling in Mouse ESCs

We next asked how Tbx6 globally regulated gene expression associated with developmental events in mouse ESCs. Among mesoderm genes upregulated by Tbx6, Mesp1 is a key transcription factor for mesoderm induction and was upregulated in both mouse ESCs and fibroblasts with Tbx6 overexpression (Figures 1A and 5D) (Chan et al., 2013). Mesp1 contains two conserved T-box consensus binding sites (TCACAC) at the enhancer region (−4 kb) and near the transcriptional start site (TSS, +0.1 kb) (Figures 5E and 5F). To determine whether Tbx6 directly bound and upregulated Mesp1 expression, we performed chromatin immunoprecipitation (ChIP)-qPCR analyses with antibodies against Tbx6-FLAG, PolII, and immunoglobulin G (IgG) in iTbx6 T-GFP mESCs. Tbx6 binding was clearly observed at the −4-kb early mesoderm enhancer region with Dox administration, whereas it was not detected at the TSS or a +1.2-kb negative-control region, which did not contain T-box-binding sites (Figure 5F). PolII binding was increased at the TSS with Dox addition, suggesting PolII-dependent Mesp1 gene transcription (Figure 5G). Thus, Tbx6 directly upregulated Mesp1 expression. We next asked how Tbx6 globally suppressed the neural program. Sox2 is a key transcription factor for neural development, and suppression of Sox2 is critical for mesoderm and endoderm induction in human PSCs (Rao et al., 2016). qRT-PCR revealed that *Sox2* was strongly

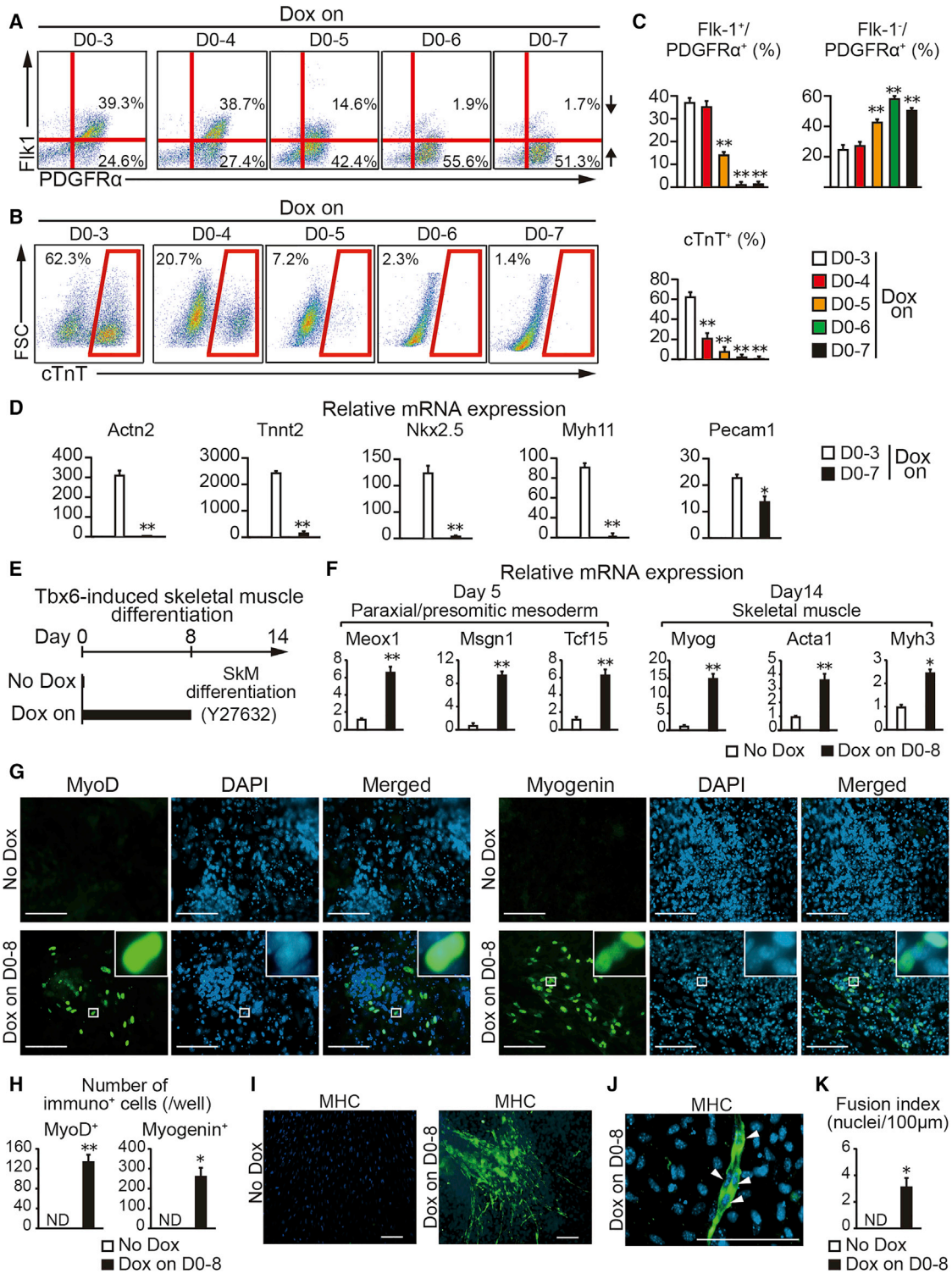

Figure 6. Continuous Tbx6 Expression Inhibited Cardiac Differentiation and Induced Paraxial Mesoderm and Skeletal Myocyte Lineages

(A–C) FACS profiles for the expression of mesoderm markers Flk-1 and PDGFRα in iTbx6 T-GFP mouse EBs at the indicated days (A). The expression of cTnT was analyzed by FACS on day 14 (B). Dox addition was started from day 0 and continued to day 7. Quantitative data are shown in (C) (n = 3, independent experiments). See also Figure 4.

(D) The mRNA expression for CM, SMC, and EC genes in iTbx6 T-GFP mESCs with Dox administration for 3 (white) and 7 days (black) (n = 3, independent experiments). Data were normalized to the values of D0–3.

(E) Scheme depicting the protocol used to induce skeletal muscle differentiation with a Dox-inducible Tbx6 expression system.

(legend continued on next page)

downregulated by Tbx6 (Figure S5C). ChIP-qPCR analyses for Tbx6 and PolII binding demonstrated that Tbx6 binding was significantly enriched on two of four T-box-containing regions (−10 and +4 kb) in the *Sox2* gene, whereas PolII binding was not enriched at the TSS after Dox administration (Figures S5D and S5E). Thus, Tbx6 directly suppressed *Sox2* expression in mouse ESCs. Moreover, Tbx6 overexpression did not induce $T^+/Sox2^+$ NMPs prior to mesoderm differentiation in iTbx6 T-GFP mESCs (Figure S5F).

We next sought to characterize the regulation of BMP, Nodal, and Wnt signaling in Tbx6-induced mesoderm in mouse ESCs. Consistent with the GO analysis, kinetic analyses for *Bmp4*, *Nodal*, and *Wnt3* mRNA expression demonstrated that *Bmp4* was rapidly and strongly upregulated after 12 hr of Dox administration, whereas *Nodal* and *Wnt3* expression were activated later (Figure 5H). These results suggest that *Bmp4* might be a primary target of Tbx6 and activation of *Nodal*/*Wnt3* was a secondary effect, consistent with the known effect of *Bmp4* to induce *Wnt* and *Nodal* during mesoderm development (Murry and Keller, 2008). Indeed, ChIP-qPCR revealed that Dox addition enriched Tbx6 and PolII binding at the *Bmp4* gene (+0.3 and +0.5 kb) and TSS, respectively (Figures S5G and S5H). Given that *Bmp4*, *Nodal*, and *Wnt3* expression were upregulated with Tbx6, we next asked whether these signaling pathways were critical for Tbx6-mediated mesoderm induction. We treated iTbx6 T-GFP mESCs with specific inhibitors for the BMP, Nodal, and Wnt signaling pathways in combination with Dox treatment. T-GFP induction was significantly reduced with these three inhibitors, suggesting that the activation of BMP, Nodal, and Wnt pathways were all required for Tbx6-mediated mesoderm induction (Figures S5I and S5J). Next, to determine whether Tbx6 induced mesoderm through non-cell-autonomous/paracrine mechanisms, we generated chimeric EBs, in which iTbx6 T-GFP mESCs (inducer, hKO^+) were mixed with parental T-GFP mESCs (responder, hKO^-). The chimeric EBs were treated with Dox without cytokines and analyzed for Flk1 and PDGFRα mesoderm induction by FACS. Dox administration induced $Flk1^+/PDGFR\alpha^+$ mesoderm in both hKO^+ and hKO^- cells; however, the induction rate was significantly higher in the inducer, suggesting that Tbx6 induced mesoderm through both cell-autonomous and non-cell-autonomous mechanisms (Figure 5I). Thus, Tbx6 directly regulates *Mesp1*, *Sox2*, and *Bmp4* expression and activates BMP/Nodal/Wnt pathways through non-cell-autonomous/paracrine mechanisms to induce mesoderm in mouse ESCs.

Prolonged Tbx6 Expression Inhibits Cardiovascular Differentiation and Induces Paraxial Mesoderm and Somite Lineages in Mouse ESCs

After transient expression of Tbx6 in nascent mesoderm, Tbx6 is continuously expressed in the paraxial/presomitic mesoderm and tail bud in mouse embryos until somite formation (Chapman et al., 1996). The ventral somite (sclerotome) generates the cartilage and vertebral column, whereas the dorsal somite (dermomyotome) forms skeletal muscles and the dermis of the back (Loh et al., 2016). However, it remains unknown whether Tbx6 expression is sufficient to induce paraxial mesoderm and somite lineages in ESCs. To address this, we continuously expressed Tbx6 in iTbx6 mESCs by prolonged Dox administration without the addition of exogenous factors (Figures 6A–6C). Remarkably, continuous Tbx6 expression decreased $Flk\text{-}1^+/PDGFR\alpha^+$ cardiogenic mesoderm and increased the $Flk\text{-}1^-/PDGFR\alpha^+$ population (presumptive paraxial mesoderm) in a time-dependent manner (Figures 6A and 6C). Analyses of multiple clonal iTbx6 mESC lines revealed that $Flk\text{-}1^-/PDGFR\alpha^+$ cells were induced from ESCs by Tbx6 in a dose-dependent manner; in addition, in the absence of Dox and exogenous factors, no mesodermal cells were induced from mouse ESCs (Figures S6A and S6B). Consistent with the induction of $Flk\text{-}1^-/PDGFR\alpha^+$ population, the paraxial/presomitic mesoderm genes (*Meox1*, *Msgn1*, and *Tcf15*) were significantly upregulated on day 5 by continuous Dox administration (Figure 6F). In contrast to the robust cardiac differentiation by transient Tbx6 expression, continuous Tbx6 expression suppressed cardiovascular differentiation in a time-dependent manner (Figures 6B–6D). Next, to determine whether prolonged Tbx6-induced mesoderm could differentiate into somite lineages, we treated the cells with the ROCK inhibitor, Y27632, to induce skeletal myocyte differentiation (Chan et al., 2016) (Figure 6E). Gene expression analyses revealed that continuous Tbx6 expression for 8 days led to the upregulation of skeletal myocyte genes (*Myog*, *Acta1*, and *Myh3*) on day 14 (Dox on D0–8, Figure 6F). Immunohistochemistry demonstrated that skeletal myoblasts characterized as $MyoD^+$ and $Myogenin^+$ were induced under the conditions of differentiation (Dox on D0–8, Figures 6G and 6J), and multinucleated myosin heavy chain $(MHC)^+$ myocytes were induced after 3 weeks of culture (Figures 6I–6K). Skeletal myocytes/myoblasts were never induced without Dox administration (No Dox). Next, to investigate whether $Flk\text{-}1^-/PDGFR\alpha^+$ mesoderm could also differentiate into other somite lineages, we treated the cells with growth and differentiation factor 5 (GDF-5; also known as BMP14), a member of the TGFβ superfamily, to induce chondrocytes (Figure S6C). qRT-PCR analyses revealed that Dox administration upregulated the expression of chondrocyte-enriched genes, *Sox9* and *Col2a1* (Dox on D0–8, Figure S6D). Safranin-O staining and immunohistochemistry for Sox9 and Col2a1 demonstrated chondrocyte induction from mouse ESCs by Tbx6 expression for 8 days (Dox on D0–8, Figures S6E and S6F). If Tbx6 was further continuously expressed, neither cardiovascular or somite lineage was induced (data not shown). Thus, prolonged Tbx6 expression inhibited cardiovascular differentiation and instead induced paraxial mesoderm and somite lineages in mouse ESCs, consistent with the kinetics of Tbx6 *in vivo*.

(F) The mRNA expression for paraxial/presomitic mesoderm and skeletal muscle genes in iTbx6 T-GFP mESCs with (black, Dox on D0-8) or without Dox (white, No Dox) (n = 3, independent experiments). Data were normalized to the values of No Dox.

(G and H) iTbx6 T-GFP mESCs were differentiated into skeletal muscle lineage under the conditions used. The Dox-treated cells (Dox on D0–8) expressed MyoD and Myogenin after 14 days (G). No $MyoD^+$ or $Myogenin^+$ cells were observed in control (No Dox) wells. Quantitative data are shown in (H).

(I–K) Immunocytochemistry for MHC after 21 days (I). Arrowheads indicate multiple nuclei in the MHC^+ myotube (J). Quantitative data are shown in (K).

All data are presented as the mean ± SD. $^{**}p < 0.01$; $^{*}p < 0.05$ versus D0–3 (C and D) or No Dox (F, H, and K). Scale bars represent 100 μm. See also Figures S6 and S7.

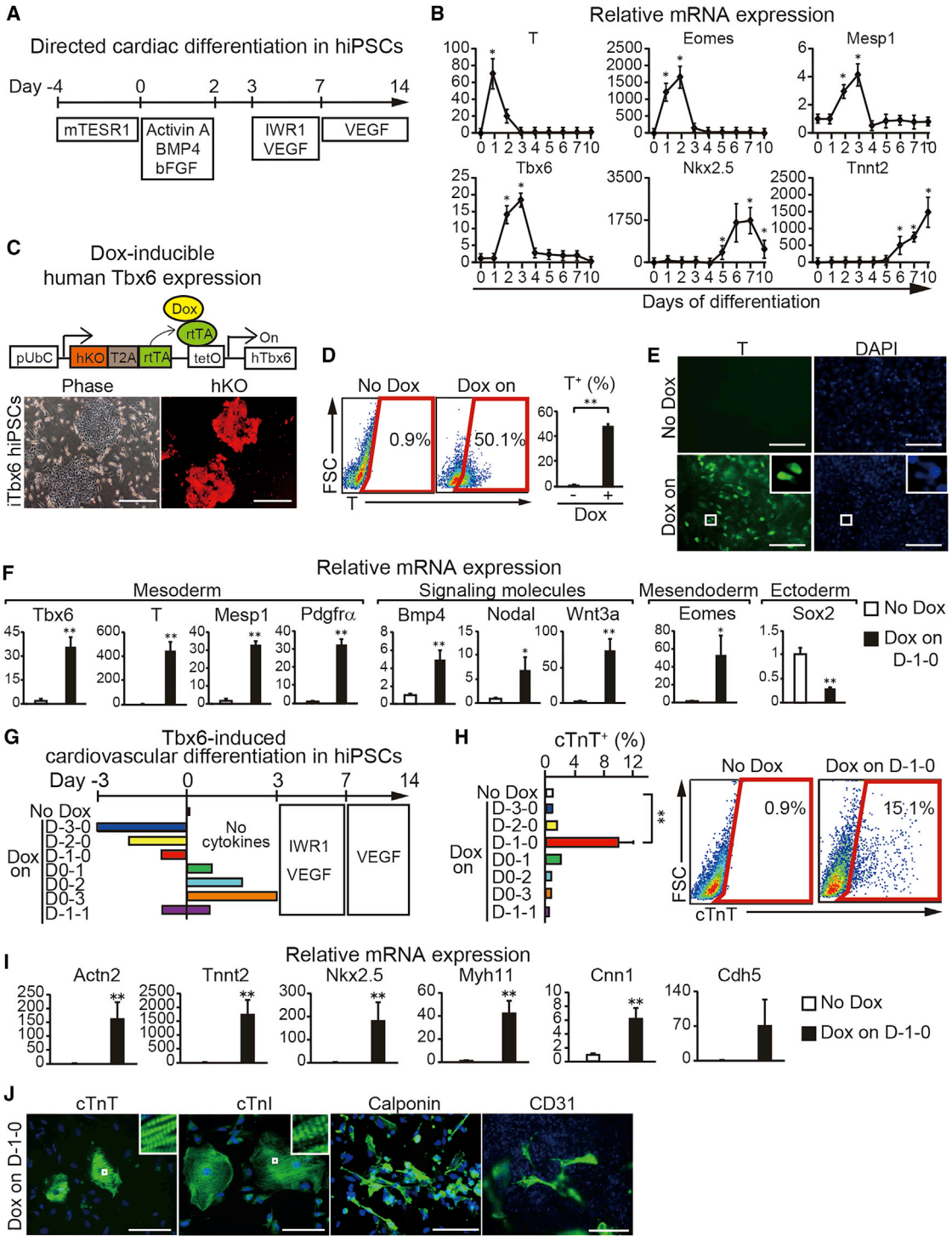

Figure 7. Transient Tbx6 Expression Induced Mesoderm and Cardiovascular Lineages in Human iPSCs

(A) Schematic representation of the directed cardiac differentiation protocol in human iPSCs.

(B) Time course of mRNA expression during hiPSC differentiation determined by qRT-PCR. Data were normalized to the values on day 0.

(C) Schematic representation of the lentiviral construct for Dox-inducible human Tbx6 expression. Clonal expansion of the iTbx6 hiPSC was confirmed by hKO expression.

(D and E) FACS analysis (D) and immunocytochemistry (E) demonstrated that T protein was expressed in the Dox-induced hiPSC nuclei on day 1 of differentiation (n = 3, independent experiments).

(F) The mRNA expression for mesoderm, signaling molecules, mesendoderm, and ectoderm genes in iTbx6 hiPSCs with (black, Dox on day −1 to 0) or without Dox (white, No Dox) in the absence of additional cytokines on day 1 (n = 3, independent experiments). Data were normalized to the values of No Dox.

(legend continued on next page)

Next, we investigated how temporal Tbx6 expression regulates mesodermal lineage specification. We analyzed the expression of *Wnt3*, *Msx1*, and *Cdx2*, which are implicated in paraxial mesoderm development (Rao et al., 2016). qRT-PCR revealed that *Wnt3* was strongly upregulated with continuous Tbx6 expression, peaking on day 5. *Msx1* and *Cdx2*, targets of Wnt signaling, were subsequently induced with prolonged Tbx6 expression, peaking on day 6 (Figure S7A). We next overexpressed Msx1 and Cdx2 in iTbx6 mouse ESCs with transient Dox administration to determine their roles in Tbx6-induced differentiation (Figure S7B). FACS analyses and immunohistochemistry revealed that overexpression of Msx1 and Cdx2 strongly inhibited cardiac differentiation, suggesting that temporal Tbx6 expression regulates cardiac versus somite lineage differentiation, at least in part, via Wnt3, Msx1, and Cdx2 expression (Figures S7C and S7D).

Transient Tbx6 Expression Induces Mesoderm and Cardiovascular Lineages in Human PSCs

Mouse and human PSCs represent different stages of development, but the signaling pathways that regulate their differentiation are similar (Kattman et al., 2011). We next investigated the role of Tbx6 in human cardiovascular differentiation using human induced PSCs (hiPSCs), 253G4. Directed cardiac differentiation using a series of multiple cytokines and small molecules sequentially specified the hiPSCs into mesoderm, CPCs, and CMs (Figure 7A). qRT-PCR revealed that *Tbx6* expression rapidly increased on day 2, one day after the induction of *T* and *Eomes* expression, and sharply decreased on day 4. This kinetics was similar to that of *Mesp1*, whereas *Nkx2.5* and *Tnnt2* were induced thereafter, suggesting that *Tbx6* was transiently induced at a mesoderm stage before CPC and CM differentiation in human PSCs (Figure 7B).

Next, we generated clonal hiPSC lines, in which human Tbx6 could be induced by Dox administration (iTbx6 hiPSCs) (Figures 7C and 7F). Without the addition of exogenous factors and Dox (No Dox), the iTbx6 hiPSCs never differentiated into T^+ mesoderm. In contrast, Dox administration alone was sufficient to induce ~50% of T^+ nascent mesoderm in the iTbx6 hiPSCs without the addition of cytokines, as shown by FACS and immunohistochemistry (Dox on, Figures 7D and 7E). Gene expression analyses revealed that mesoderm, signaling molecules, and mesendoderm-related genes, such as *T*, *Mesp1*, *Pdgfra*, *Wnt3a*, *Bmp4*, *Nodal*, and *Eomes*, were greatly upregulated with Dox addition, whereas the neural transcription factor, *Sox2*, was downregulated in the hiPSCs, similar to mouse ESCs (Figure 7F). We next asked whether Tbx6-induced mesoderm could differentiate into cardiovascular lineages in hiPSCs. To determine the appropriate timing of Dox addition for cardiac induction, we sequentially treated the hiPSCs with Dox and analyzed cardiac induction by FACS after 14 days of differentiation (Figure 7G). For the iTbx6 hiPSCs, Dox administration from days −1 to 0 was found to be optimal to induce 15% of $cTnT^+$ cells, which represents, however, a lower efficiency than that in iTbx6 mESCs (Figures 4I and 7H). The Tbx6-induced human CMs beat synchronously in culture (Video S2). qRT-PCR and immunostaining demonstrated that Tbx6-induced mesoderm differentiated into all three cardiovascular lineages, whereas no cardiovascular differentiation was observed without Dox treatment (Figures 7I and 7J). Thus, transient Tbx6 expression also induced mesoderm and cardiovascular lineages in human PSCs, similar to the results in mouse ESCs.

DISCUSSION

Tbx6 has been regarded as a marker of paraxial mesoderm and implicated mainly in somite development in mammals (Chapman and Papaioannou, 1998; Loh et al., 2016). Here, we reveal an essential and unexpected function of Tbx6 in nascent mesoderm induction and subsequent lineage diversification into cardiovascular and somite lineages in PSCs regulated by its temporal expression. Transient Tbx6 expression induced cardiac/lateral mesoderm and cardiovascular lineages, while continuous Tbx6 expression suppressed cardiac differentiation and induced paraxial/presomitic mesoderm and somite lineage specification.

We screened key regulators for mesoderm induction in mouse fibroblasts with the direct reprogramming approach. Fibroblasts are efficiently transduced with retroviral vectors without gene silencing and are easier and cheaper to culture than PSCs. We found that Tbx6 induced a nascent mesoderm-like program in fibroblasts by screening of 58 factors. Although the precise mechanisms remain undetermined, we found that Tbx6 induced mesoderm-related genes but not genes related to differentiated cardiovascular cells or skeletal myocytes, suggesting that Tbx6 induced and maintained a mesodermal program in fibroblasts. Consistent with our results, Tbx6 is expressed in nascent mesoderm, and subsequently in paraxial mesoderm, but not in somites or other differentiated derivatives *in vivo* (Chapman et al., 1996). These results suggest that Tbx6 induces the mesoderm program but that suppression of Tbx6 may be a prerequisite for mesoderm differentiation. Given that the gene regulatory networks of programming (differentiation) and reprogramming are similar, the direct reprogramming-based approach we describe here might be applicable in general for the identification of new key regulators and their functions in cell-fate decision.

$Tbx6^+$ nascent mesoderm is a transient population, arising early in gastrulation, but the nature of this population remained unclear, because the genome-wide transcriptional profile has not been determined owing to the small sample size. We revealed a detailed molecular signature of $Tbx6^+$ nascent mesoderm cells in E7.0 mouse embryos by analyzing single-cell RNA-seq. Single-cell RNA-seq demonstrated that the $Tbx6^+$ mesoderm progenitors were a highly homogeneous population, expressing not only nascent mesoderm genes but

(G) Scheme depicting the protocol used to evaluate the effects of Tbx6 expression on Dox-induced cardiovascular induction in hiPSCs.
(H) FACS profiles for the expression of cTnT in hiPSCs with the indicated Dox protocols (G) and analyzed on day 14.
(I and J) The mRNA expression and immunocytochemistry analyses demonstrated that iTbx6 hiPSCs were differentiated into CMs, SMCs, and ECs with Dox administration for 1 day (I). Data were analyzed on day 14 and normalized to the values of No Dox (n = 3, independent experiments), and representative images are shown in (J).
All data are presented as the mean ± SD. $^{**}p < 0.01$; $^{*}p < 0.05$ versus day 0 (B) or No Dox (D, F, H, and I). Scale bars represent 100 μm.

also lateral/cardiac mesoderm and early CPC genes, suggesting they might be transitioning from nascent mesoderm to cardiovascular lineages. We also found that Tbx6 was expressed in the mesoderm before cardiac progenitors and cardiac differentiation in PSC-based directed cardiac differentiation. Thus, our characterization of the Tbx6$^+$ nascent mesoderm in single-cell analyses revealed a connection between early Tbx6 expression and cardiovascular lineage differentiation, and such single-cell analyses may change our current view of lineage specification during development. Consistent with our results, Concepcion et al. have recently reported that the progeny of the Tbx6$^+$ nascent mesoderm was distributed not only in the paraxial mesoderm and somites, but also in the lateral/cardiac mesoderm, heart, and blood vessel endothelium by analyzing Tbx6-creERT2 lineage tracing mice (Concepcion et al., 2017).

Although Tbx6 has been regarded to function mainly in somite development in mammals, Tbx6 is critical for cardiac mesoderm formation and cardiogenesis in lower organisms. *Drosophila* lacking the Tbx6 homolog Dorsocross do not form a dorsal vessel, which is equivalent to the heart. In *Ciona intestinalis*, the ortholog of Tbx6 acts upstream of Mesp to form the cardiac mesoderm (Christiaen et al., 2009; Reim and Frasch, 2005; Satou et al., 2004). In mammals, Tbx6 mutant mice show dramatic defects in somite formation and die at mid-gestation. However, they also exhibit cardiovascular defects such as a lack of heartbeats, abnormal heart looping, and vascular hemorrhages, although the underlying mechanisms of these cardiovascular defects remain poorly understood (Chapman and Papaioannou, 1998). In humans, heart abnormalities such as ventricular septal defects were recently reported in two out of nine Japanese congenital scoliosis patients with *TBX6* mutations (Takeda et al., 2017). Consistent with these cardiovascular defects in mammals, we found that KO of the Tbx6 gene inhibited mesoderm specification and cardiovascular differentiation in mouse ESCs. A previous study showed that Tbx6 KO mouse ESCs differentiated into contractile EBs similar to WT ESCs under fetal bovine serum (FBS)-mediated hanging drop differentiation; however, this may underestimate the effect of Tbx6 on cardiac differentiation, as the authors did not quantify the efficiency of mesoderm and cardiovascular differentiation using FACS or qRT-PCR (Chapman et al., 2003). Thus, our study revealed an essential and unappreciated function of Tbx6 in mesoderm and cardiovascular specification conserved from lower organisms to mammals. Although there are cardiovascular defects in Tbx6 KO mice, myocardial tissues develop in the mutant mice. It is conceivable that the redundancy with other T-box genes (*T*, *Eomes*, *Mesp1*) may compensate for the cardiac phenotype in Tbx6 KO mice. Indeed, we found that expression of *T*, *Mesp1*, and *Eomes*, as well as cardiac differentiation, was suppressed but not completely ablated in Tbx6 KO ESCs. Thus, Tbx6 is important but not required for mesoderm formation and cardiac development in mammals.

We also found that Tbx6 overexpression, in the absence of exogenous cytokines, was sufficient to induce nascent mesoderm that subsequently differentiated into cardiovascular lineages in mouse and human PSCs. Although the expression and function of Tbx6 were similar in mice and humans, there were some notable differences. The timing and duration of Tbx6 expression for optimal cardiac differentiation differed, and the efficiency of T$^+$ mesoderm and CM induction was substantially lower in humans. Some of these differences may be attributable to distinct pluripotent states, endogenous signaling, and transgene expression between human and mouse PSCs (Kattman et al., 2011). Nonetheless, these results further demonstrate an evolutionarily conserved role of Tbx6 in mesoderm specification and subsequent cardiovascular differentiation in mammals. Consistent with our findings, Gavrilov et al. reported the positive effects of Tbx6 in promoting cardiac differentiation and repressing neural differentiation using the mouse embryonic carcinoma P19CL6 cell line (Gavrilov et al., 2012).

Mechanistically, Tbx6 induced mesoderm by directly activating *Mesp1* and *BMP4* and repressing *Sox2*, and presumably, indirectly inducing *Wnt* and *Nodal* expression. Activation of BMP4, Nodal, and Wnt pathways by Tbx6 expression non-cell-autonomously induces mesoderm specification, which may in turn upregulate *Tbx6* expression and create a positive feedback loop for robust induction of mesoderm. We also found that prolonged *Tbx6* expression continuously upregulated *Wnt3* expression after mesoderm induction, which subsequently induced *Msx1* and *Cdx2* expression and interfered with cardiac differentiation. Such mechanisms may be responsible for Tbx6-mediated mesoderm induction and subsequent lineage diversification. Although prolonged Tbx6 expression-induced mesoderm differentiated into skeletal myocytes with the ROCK inhibitor, other protocols were not as efficient as the ROCK inhibitor treatment in our ESC lines (data not shown) (Chal and Pourquié, 2017). Different differentiation efficacy among protocols may be attributable to endogenous signaling and Tbx6 transgene expression in our ESCs.

Collectively, we demonstrate that Tbx6 has dramatic effects on nascent mesoderm induction and subsequent lineage specification in PSCs. Our results provide the basis for understanding mesoderm development as well as for the generation of desired cell types for regenerative medicine in the future.

STAR★METHODS

Detailed methods are provided in the online version of this paper and include the following:

- KEY RESOURCES TABLE
- CONTACT FOR REAGENT AND RESOURCE SHARING
- EXPERIMENTAL MODEL AND SUBJECT DETAILS
  - Generation of Mesp1-GFP mice
  - Mouse ESCs
  - Human PSCs
- METHOD DETAILS
  - Retroviral Infection and Cell Culture
  - Histology and Cell Counting
  - Flow Cytometry and Cell Sorting
  - Quantitative RT-PCR
  - Mouse ESC Differentiation
  - Generation of Tbx6 KO ESCs
  - Lentiviral Infection and Generation of iTbx6 PSCs
  - Human PSC Differentiation
  - Microarray Analyses
  - Bioinformatics Analysis
  - Single-cell RNA-seq Analyses

SUPPLEMENTAL INFORMATION

Supplemental Information includes seven figures, two tables, and two videos and can be found with this article online at https://doi.org/10.1016/j.stem.2018.07.001.

ACKNOWLEDGMENTS

We thank B. Göttgens for permission to use their single-cell RNA-seq data in mouse embryos. We thank Y. Yasuhiko for providing the pCS2+3×FLAG Tbx6 plasmid, G. Keller for providing T-GFP ESCs, and S. Yamanaka for providing the hiPSC line (253G4). M. Ieda was supported by research grants from the Research Center Network for Realization of Regenerative Medicine, Japan Agency for Medical Research and Development (AMED), the Japan Society for the Promotion of Science (JSPS) (17H04179), Senshin Medical Research Foundation, Takeda Science Foundation, and Daiichi-Sankyo Foundation of Life Science, and T.S. was supported by research grants from JSPS (16K19426 and 18K08114), Japan Heart Foundation Research Grant, Nakatomi Foundation, Miyata Cardiac Research Promotion Foundation, Keio University Medical Science Fund, and Keio University Grant-in-Aid for Encouragement of Young Medical Scientists (02-002-0022 and 02-002-0017).

AUTHOR CONTRIBUTIONS

T.S. and M. Ieda designed the experiments. M. Isomi, N.M., H.K., S.H., S.K., F.T., H.T., S.T., J.F., Y.K., Y.W.I., K.M., M.O., P.A., H.N., and H.U. performed the experiments. T.S., H.M., N.G., K.S., C.K., and K.F. analyzed the data. T.S. and M. Ieda wrote the paper.

DECLARATION OF INTERESTS

T.S., M. Isomi, N.G., and M. Ieda are inventors on patent applications describing the Tbx6-induced reprogramming and differentiation into cardiac progenitors and cardiomyocytes.

Received: December 15, 2017
Revised: May 8, 2018
Accepted: July 2, 2018
Published: August 9, 2018

REFERENCES

Burridge, P.W., Matsa, E., Shukla, P., Lin, Z.C., Churko, J.M., Ebert, A.D., Lan, F., Diecke, S., Huber, B., Mordwinkin, N.M., et al. (2014). Chemically defined generation of human cardiomyocytes. Nat. Methods *11*, 855–860.

Chal, J., and Pourquié, O. (2017). Making muscle: Skeletal myogenesis *in vivo* and *in vitro*. Development *144*, 2104–2122.

Chal, J., Oginuma, M., Al Tanoury, Z., Gobert, B., Sumara, O., Hick, A., Bousson, F., Zidouni, Y., Mursch, C., Moncuquet, P., et al. (2015). Differentiation of pluripotent stem cells to muscle fiber to model Duchenne muscular dystrophy. Nat. Biotechnol. *33*, 962–969.

Chan, S.S., Shi, X., Toyama, A., Arpke, R.W., Dandapat, A., Iacovino, M., Kang, J., Le, G., Hagen, H.R., Garry, D.J., and Kyba, M. (2013). Mesp1 patterns mesoderm into cardiac, hematopoietic, or skeletal myogenic progenitors in a context-dependent manner. Cell Stem Cell *12*, 587–601.

Chan, S.S., Hagen, H.R., Swanson, S.A., Stewart, R., Boll, K.A., Aho, J., Thomson, J.A., and Kyba, M. (2016). Development of bipotent cardiac/skeletal myogenic progenitors from MESP1+ mesoderm. Stem Cell Reports *6*, 26–34.

Chapman, D.L., and Papaioannou, V.E. (1998). Three neural tubes in mouse embryos with mutations in the T-box gene Tbx6. Nature *391*, 695–697.

Chapman, D.L., Agulnik, I., Hancock, S., Silver, L.M., and Papaioannou, V.E. (1996). Tbx6, a mouse T-Box gene implicated in paraxial mesoderm formation at gastrulation. Dev. Biol. *180*, 534–542.

Chapman, D.L., Cooper-Morgan, A., Harrelson, Z., and Papaioannou, V.E. (2003). Critical role for Tbx6 in mesoderm specification in the mouse embryo. Mech. Dev. *120*, 837–847.

Christiaen, L., Stolfi, A., Davidson, B., and Levine, M. (2009). Spatio-temporal intersection of Lhx3 and Tbx6 defines the cardiac field through synergistic activation of Mesp. Dev. Biol. *328*, 552–560.

Concepcion, D., Washkowitz, A.J., DeSantis, A., Ogea, P., Yang, J.I., Douglas, N.C., and Papaioannou, V.E. (2017). Cell lineage of timed cohorts of *Tbx6*-expressing cells in wild-type and *Tbx6* mutant embryos. Biol. Open *6*, 1065–1073.

Cong, L., Ran, F.A., Cox, D., Lin, S., Barretto, R., Habib, N., Hsu, P.D., Wu, X., Jiang, W., Marraffini, L.A., and Zhang, F. (2013). Multiplex genome engineering using CRISPR/Cas systems. Science *339*, 819–823.

Costello, I., Pimeisl, I.M., Dräger, S., Bikoff, E.K., Robertson, E.J., and Arnold, S.J. (2011). The T-box transcription factor Eomesodermin acts upstream of Mesp1 to specify cardiac mesoderm during mouse gastrulation. Nat. Cell Biol. *13*, 1084–1091.

Craft, A.M., Ahmed, N., Rockel, J.S., Baht, G.S., Alman, B.A., Kandel, R.A., Grigoriadis, A.E., and Keller, G.M. (2013). Specification of chondrocytes and cartilage tissues from embryonic stem cells. Development *140*, 2597–2610.

Gadue, P., Huber, T.L., Paddison, P.J., and Keller, G.M. (2006). Wnt and TGF-beta signaling are required for the induction of an in vitro model of primitive streak formation using embryonic stem cells. Proc. Natl. Acad. Sci. USA *103*, 16806–16811.

Gavrilov, S., Nuhrenberg, T.G., Ashton, A.W., Peng, C.F., Moore, J.C., Konstantinidis, K., Mummery, C.L., and Kitsis, R.N. (2012). Tbx6 is a determinant of cardiac and neural cell fate decisions in multipotent P19CL6 cells. Differentiation *84*, 176–184.

Gouti, M., Tsakiridis, A., Wymeersch, F.J., Huang, Y., Kleinjung, J., Wilson, V., and Briscoe, J. (2014). In vitro generation of neuromesodermal progenitors reveals distinct roles for wnt signalling in the specification of spinal cord and paraxial mesoderm identity. PLoS Biol. *12*, e1001937.

Hemmi, N., Tohyama, S., Nakajima, K., Kanazawa, H., Suzuki, T., Hattori, F., Seki, T., Kishino, Y., Hirano, A., Okada, M., et al. (2014). A massive suspension culture system with metabolic purification for human pluripotent stem cell-derived cardiomyocytes. Stem Cells Transl. Med. *3*, 1473–1483.

Ieda, M., Fu, J.D., Delgado-Olguin, P., Vedantham, V., Hayashi, Y., Bruneau, B.G., and Srivastava, D. (2010). Direct reprogramming of fibroblasts into functional cardiomyocytes by defined factors. Cell *142*, 375–386.

Islas, J.F., Liu, Y., Weng, K.C., Robertson, M.J., Zhang, S., Prejusa, A., Harger, J., Tikhomirova, D., Chopra, M., Iyer, D., et al. (2012). Transcription factors ETS2 and MESP1 transdifferentiate human dermal fibroblasts into cardiac progenitors. Proc. Natl. Acad. Sci. USA *109*, 13016–13021.

Kattman, S.J., Huber, T.L., and Keller, G.M. (2006). Multipotent flk-1+ cardiovascular progenitor cells give rise to the cardiomyocyte, endothelial, and vascular smooth muscle lineages. Dev. Cell *11*, 723–732.

Kattman, S.J., Witty, A.D., Gagliardi, M., Dubois, N.C., Niapour, M., Hotta, A., Ellis, J., and Keller, G. (2011). Stage-specific optimization of activin/nodal and BMP signaling promotes cardiac differentiation of mouse and human pluripotent stem cell lines. Cell Stem Cell *8*, 228–240.

Kawamoto, S., Niwa, H., Tashiro, F., Sano, S., Kondoh, G., Takeda, J., Tabayashi, K., and Miyazaki, J. (2000). A novel reporter mouse strain that expresses enhanced green fluorescent protein upon Cre-mediated recombination. FEBS Lett. *470*, 263–268.

Kurita, R., Suda, N., Sudo, K., Miharada, K., Hiroyama, T., Miyoshi, H., Tani, K., and Nakamura, Y. (2013). Establishment of immortalized human erythroid progenitor cell lines able to produce enucleated red blood cells. PLoS ONE *8*, e59890.

Lee, T.I., Johnstone, S.E., and Young, R.A. (2006). Chromatin immunoprecipitation and microarray-based analysis of protein location. Nat. Protoc. *1*, 729–748.

Lian, X., Hsiao, C., Wilson, G., Zhu, K., Hazeltine, L.B., Azarin, S.M., Raval, K.K., Zhang, J., Kamp, T.J., and Palecek, S.P. (2012). Robust cardiomyocyte differentiation from human pluripotent stem cells via temporal modulation of canonical Wnt signaling. Proc. Natl. Acad. Sci. USA *109*, E1848–E1857.

Liu, Y., Chen, L., Diaz, A.D., Benham, A., Xu, X., Wijaya, C.S., Fa'ak, F., Luo, W., Soibam, B., Azares, A., et al. (2016). Mesp1 marked cardiac progenitor cells repair infarcted mouse hearts. Sci. Rep. *6*, 31457.

Loh, K.M., Chen, A., Koh, P.W., Deng, T.Z., Sinha, R., Tsai, J.M., Barkal, A.A., Shen, K.Y., Jain, R., Morganti, R.M., et al. (2016). Mapping the pairwise choices leading from pluripotency to human bone, heart, and other mesoderm cell types. Cell *166*, 451–467.

Muraoka, N., Yamakawa, H., Miyamoto, K., Sadahiro, T., Umei, T., Isomi, M., Nakashima, H., Akiyama, M., Wada, R., Inagawa, K., et al. (2014). MiR-133 promotes cardiac reprogramming by directly repressing Snai1 and silencing fibroblast signatures. EMBO J. *33*, 1565–1581.

Murry, C.E., and Keller, G. (2008). Differentiation of embryonic stem cells to clinically relevant populations: Lessons from embryonic development. Cell *132*, 661–680.

Paige, S.L., Thomas, S., Stoick-Cooper, C.L., Wang, H., Maves, L., Sandstrom, R., Pabon, L., Reinecke, H., Pratt, G., Keller, G., et al. (2012). A temporal chromatin signature in human embryonic stem cells identifies regulators of cardiac development. Cell *151*, 221–232.

Ran, F.A., Hsu, P.D., Wright, J., Agarwala, V., Scott, D.A., and Zhang, F. (2013). Genome engineering using the CRISPR-Cas9 system. Nat. Protoc. *8*, 2281–2308.

Rao, J., Pfeiffer, M.J., Frank, S., Adachi, K., Piccini, I., Quaranta, R., Araúzo-Bravo, M., Schwarz, J., Schade, D., Leidel, S., et al. (2016). Stepwise Clearance of Repressive Roadblocks Drives Cardiac Induction in Human ESCs. Cell Stem Cell *18*, 341–353.

Reim, I., and Frasch, M. (2005). The Dorsocross T-box genes are key components of the regulatory network controlling early cardiogenesis in Drosophila. Development *132*, 4911–4925.

Sadahiro, T., Yamanaka, S., and Ieda, M. (2015). Direct cardiac reprogramming: Progress and challenges in basic biology and clinical applications. Circ. Res. *116*, 1378–1391.

Saga, Y., Miyagawa-Tomita, S., Takagi, A., Kitajima, S., Miyazaki, Ji., and Inoue, T. (1999). MesP1 is expressed in the heart precursor cells and required for the formation of a single heart tube. Development *126*, 3437–3447.

Satou, Y., Imai, K.S., and Satoh, N. (2004). The ascidian Mesp gene specifies heart precursor cells. Development *131*, 2533–2541.

Scialdone, A., Tanaka, Y., Jawaid, W., Moignard, V., Wilson, N.K., Macaulay, I.C., Marioni, J.C., and Göttgens, B. (2016). Resolving early mesoderm diversification through single-cell expression profiling. Nature *535*, 289–293.

Takeda, K., Kou, I., Kawakami, N., Iida, A., Nakajima, M., Ogura, Y., Imagawa, E., Miyake, N., Matsumoto, N., Yasuhiko, Y., et al.; Japan Early Onset Scoliosis Research Group (2017). Compound heterozygosity for null mutations and a common hypomorphic risk haplotype in TBX6 causes congenital scoliosis. Hum. Mutat. *38*, 317–323.

Takemoto, T., Uchikawa, M., Yoshida, M., Bell, D.M., Lovell-Badge, R., Papaioannou, V.E., and Kondoh, H. (2011). Tbx6-dependent Sox2 regulation determines neural or mesodermal fate in axial stem cells. Nature *470*, 394–398.

Wamstad, J.A., Alexander, J.M., Truty, R.M., Shrikumar, A., Li, F., Eilertson, K.E., Ding, H., Wylie, J.N., Pico, A.R., Capra, J.A., et al. (2012). Dynamic and coordinated epigenetic regulation of developmental transitions in the cardiac lineage. Cell *151*, 206–220.

Wardle, F.C., and Papaioannou, V.E. (2008). Teasing out T-box targets in early mesoderm. Curr. Opin. Genet. Dev. *18*, 418–425.

Weidgang, C.E., Russell, R., Tata, P.R., Kühl, S.J., Illing, A., Müller, M., Lin, Q., Brunner, C., Boeckers, T.M., Bauer, K., et al. (2013). TBX3 directs cell-fate decision toward mesendoderm. Stem Cell Reports *1*, 248–265.

Yamakawa, H., Muraoka, N., Miyamoto, K., Sadahiro, T., Isomi, M., Haginiwa, S., Kojima, H., Umei, T., Akiyama, M., Kuishi, Y., et al. (2015). Fibroblast growth factors and vascular endothelial growth factor promote cardiac reprogramming under defined conditions. Stem Cell Reports *5*, 1128–1142.

Ying, Q.L., Wray, J., Nichols, J., Batlle-Morera, L., Doble, B., Woodgett, J., Cohen, P., and Smith, A. (2008). The ground state of embryonic stem cell self-renewal. Nature *453*, 519–523.

STAR★METHODS

KEY RESOURCES TABLE

REAGENT or RESOURCE	SOURCE	IDENTIFIER
Antibodies		
Mouse monoclonal anti-GFP	Molecular Probes	Cat# A-11120; RRID:AB_221568
Rabbit polyclonal anti-GFP	MBL	Cat# 598S; RRID:AB_591816
Goat polyclonal anti-Brachyury	R&D systems	Cat# AF2085; RRID:AB_2200235
Mouse monoclonal anti-αactinin	Sigma-Aldrich	Cat# A7811; RRID:AB_476766
Rabbit polyclonal anti- Myosin IgG smooth muscle	Biomedical technologies inc	Cat# BT-562; RRID:AB_10013421
Mouse monoclonal anti- Troponin T	Lab Vision	Cat# MS-295-P1; RRID:AB_61808
Rabbit monoclonal anti-Calponin	Abcam	Cat# ab46794; RRID:AB_2291941
Rat monoclonal anti-CD31	BD Biosciences	Cat# 550274; RRID:AB_393571
Mouse monoclonal anti-FLAG M2	Sigma-Aldrich	Cat# F3165; RRID:AB_259529
Mouse monoclonal anti-RNA polymerase II	Abcam	Cat# ab5408; RRID:AB_304868
Rabbit polyclonal anti-Sox2	Abcam	Cat# ab97959; RRID:AB_2341193
Mouse monoclonal anti-MyoD	BD Biosciences	Cat# 554130; RRID:AB_395255
Mouse monoclonal anti-Myogenin	BD Biosciences	Cat# 556358; RRID:AB_396383
Mouse monoclonal anti-Myosin Heavy Chain	R and D Systems	Cat# MAB4470; RRID:AB_1293549
Mouse monoclonal anti-Collagen II	Abcam	Cat# ab185430
Mouse monoclonal anti-Sox9	Santa Cruz	Cat# sc-166505; RRID:AB_2255399
Alexa Fluor 488 goat anti-rabbit IgG	Thermo Fisher Scientific	Cat# A11008; RRID: AB_143165
Alexa Fluor 488 goat anti-mouse IgG	Thermo Fisher Scientific	Cat# A11001; RRID: AB_2534069
Alexa Fluor 488 goat anti-rat IgG	Thermo Fisher Scientific	Cat# A-11006; RRID:AB_2534074
Alexa Fluor 488 goat anti-goat IgG	Thermo Fisher Scientific	Cat# A-11055; RRID:AB_2534102
Alexa Fluor 546 goat anti-rabbit IgG	Thermo Fisher Scientific	Cat# A11010; RRID: AB_143156
Chemicals, Peptides, and Recombinant Proteins		
Leukemia inhibitory factor	Millipore	Cat# ESG1106
CHIR99021	Selleckchem	S1263
PD325901	Selleckchem	S1036
B27 supplements	Invitrogen	17504-044
N2 supplements	Invitrogen	17502-048
Recombinant human Activin A	R&D systems	338-AC
Recombinant human BMP4	R&D systems	314-BP
Recombinant human VEGF	R&D systems	293-VE
Recombinant human bFGF	R&D systems	233-FB
Recombinant human FGF10	R&D systems	345-FG
Dorsomorphin	Sigma-Aldrich	P5499
SB431542	Wako	192-16541
IWR-1	Sigma-Aldrich	I0161
Doxycycline hyclate	Sigma-Aldrich	D9891
Y27632	Wako	253-00513
GDF-5	Prospec	Cyt-941
Critical Commercial Assays		
FastStart Universal Probe Master	Roche	4914058001
Deposited Data		
Raw and analyzed data	This paper	GEO: GSE89820

(*Continued on next page*)

Continued

REAGENT or RESOURCE	SOURCE	IDENTIFIER
Experimental Models: Cell Lines		
Mouse: $T^{GFP/+}$ ESCs	Kattman et al., 2006	N/A
Mouse: E14 ESC	Laboratory of D. Srivastava	RRID:CVCL_C320
Mouse: Tbx6 KO E14 ESC	This paper	N/A
Mouse: iTbx6 T-GFP ESC	This paper	N/A
Human: 253G4 iPSC	Laboratory of S.Yamanaka	RRID:CVCL_T792
Human: iTbx6 253G4 iPSC	This paper	N/A
Experimental Models: Organisms/Strains		
Mouse: GFPfl/fl: Mesp1-Cre	Saga et al., 1999	N/A
Mouse: ICR	CLEA Japan	N/A
Oligonucleotides		
CRISPR/Cas9 Target Site, Homology Arms, and PCR Primers - See Table S1	This paper	N/A
Primers for ChIP analysis - See Table S2	This paper	N/A
Recombinant DNA		
pMXs-GW	Laboratory of S.Yamanaka	N/A
CSIV-TRE-RfA-UbC-KT	RIKEN BSI	N/A
CSII-CMV-RfaA	RIKEN BSI	N/A
pCMV-VSV-G-RSV-Rev	RIKEN BSI	N/A
pX330-U6-Chimeric_BB-CBh-hSpCas9	Cong et al., 2013	Addgene #42230
Software and Algorithms		
FlowJo software	Tomy Digital Biology	FlowJo 7.6.5
ImageJ	NIH	https://imagej.nih.gov/ij/

CONTACT FOR REAGENT AND RESOURCE SHARING

Further requests for reagents may be directed to, and will be fulfilled by, the Lead Contact Masaki Ieda (mieda@md.tsukuba.ac.jp).

EXPERIMENTAL MODEL AND SUBJECT DETAILS

Generation of Mesp1-GFP mice

Mesp1-GFP mice were obtained by crossing Mesp1-Cre mice and CAG-CAT-EGFP (GFP-flox) reporter mice (Kawamoto et al., 2000; Saga et al., 1999). The transgenic mice were maintained on a mixed ICR background. Eight-week-old male ICR (Jcl:ICR) mice were purchased from CLEA Japan (Tokyo, Japan). No health problems were observed in the transgenic mice, and all the animals were experimentally and drug-naive before use. All animals were group-housed and bred in a dedicated husbandry SPF facility with 12 h/12 h light-dark cycles, had *ad libitum* access to food and water, and were monitored daily. Their health status was routinely checked to maintain the SPF grade. Animals subjected to surgical procedures were moved to a satellite SPF facility with the same conditions. The Keio University Ethics Committee for Animal Experiments approved all experiments in this study.

Mouse ESCs

Mouse E14 and T-GFP ESCs were kindly provided by Dr. Deepak Srivastava and Dr. Gordon Keller, respectively. E14 and T-GFP mESCs were maintained in a modified feeder-free culture system (Gadue et al., 2006; Ying et al., 2008). The culture medium consisted of Glasgow Minimum Essential Medium (Sigma-Aldrich, G5154) supplemented with 10% characterized fetal bovine serum (Thermo Scientific, SH30071.03), 1% non-essential amino acids (Invitrogen, M7145), 1% penicillin/streptomycin (Invitrogen, 15070063), 2 mM GlutaMAX (Invitrogen, 35050-061), 0.1 mM mercaptoethanol (Sigma-Aldrich, 21985), 200 U/mL leukemia inhibitory factor (Millipore, ESG1106), 3 μM CHIR99021 (Selleckchem, S1263), and 1 μM PD0325901 (Selleckchem, S1036), using standard procedures.

Human PSCs

The hiPSC line (253G4) was obtained from the Center for iPSC Research and Application, Kyoto University. The hiPSCs were maintained as described previously (Hemmi et al., 2014). Briefly, we maintained hiPSCs on SNL feeder cells in DMEM/F-12 and GlutaMAX (Invitrogen, 10565-018) supplemented with 20% KO serum replacement (Invitrogen, 10828028), 0.1 mM non-essential amino acids, 0.1 mM β-mercaptoethanol, and 5 ng/mL bFGF.

METHOD DETAILS

Retroviral Infection and Cell Culture

Mouse embryonic fibroblast (MEF) isolation, generation of pMXs retroviral vectors, and transduction with retroviruses have been described previously (Ieda et al., 2010; Muraoka et al., 2014; Yamakawa et al., 2015). In brief, we generated retroviral vectors by subcloning human cDNA (HuPEX, AIST) into the pMXs-Gw plasmid using the Gateway system (Invitrogen). pMX vectors were transfected into Plat-E cells using Fugene 6 (Promega, E2691) to generate retroviruses. MEFs were transduced with the retrovirus as indicated. The medium was replaced with medium containing Dulbecco's modified Eagle's medium (Wako, 044-29765) and 10% FBS (Thermo Scientific, SV30014.03) after 24 h of infection.

Histology and Cell Counting

Cells were fixed in 4% PFA for 15 min at room temperature, blocked with 5% normal goat serum blocking solution (Vector Laboratories, S-1000), and incubated with primary antibodies against Calponin (Abcam, ab46794), cTnT (Thermo Scientific, MS-295-P1), GFP (MBL, 598), CD31 (R&D systems, 550274), Col2a1 (Abcam, ab185430), sarcomeric α-actinin (Sigma-Aldrich, 111M4845), MyoD (BD PharMingen, 554130), Myogenin (BD PharMingen, 556358), MHC (R&D systems, MAB4470), Sox2 (Abcam, ab97959), Sox9 (Santa Cruz, sc-166505), and T (R&D systems, AF2085). Cells were then incubated with secondary antibodies conjugated with Alexa Fluor 488 or 546, followed by DAPI (Invitrogen, D1306) counterstaining. The numbers of cells immunopositive for Calponin, CD31, α-actinin, MyoD and Myogenin were counted in all fields per well from at least three independent experiments. The measurements and calculations were conducted in a blinded manner. The fusion index was determined as previously described (Chal et al., 2015). Briefly, we manually counted the number of nuclei in the MHC-positive myofibers at 40 × magnification, measured the length of the myocytes with ImageJ software, and determined the number of nuclei per 100 μm of cell length. The fusion index was calculated in 10 randomly selected fields per well in at least three independent experiments. The measurements and calculations were conducted in a blinded manner. For safranin-O staining, cells were fixed in 4% PFA for 10 min at room temperature, washed twice in PBS, treated with 1 M acetic acid for 15 s, stained with 1% safranin-O for 10 min, and washed with PBS.

Flow Cytometry and Cell Sorting

Embryoid bodies (EBs) and cells were trypsinized and harvested, and single-cell suspensions were analyzed or sorted using a FACS Aria III instrument (BD Biosciences). The cells were stained for the presence of appropriate markers. Cells were stained with the following antibodies: anti-mouse Flk1 conjugated with APC (eBioscience, 17-5821) and anti-mouse PDGFRα (CD140a) conjugated with BV421 (BD Biosciences, 562774). For cTnT expression, cells were fixed with 4% paraformaldehyde (PFA) for 15 min, permeabilized with saponin (Sigma-Aldrich, 47036-250G-F), stained with anti-cTnT (Thermo Scientific, MS-295-P1) antibody, followed by incubation with secondary antibody conjugated with Alexa Fluor 488 or 647 (Invitrogen). Data were analyzed with the FlowJo software (Tomy Digital Biology). Negative controls included cells stained with isotype control antibodies.

Quantitative RT-PCR

Total RNA was prepared using the RNA Cell Miniprep System (Promega, Z6012). RNA (1 μg) was reverse transcribed into cDNA using Oligo (dT) and SuperScript II Reverse Transcriptase (Invitrogen, 18064-014). qRT-PCR was performed using the StepOnePlus Real-Time PCR system with the following TaqMan probes (Applied Biosystems). Mouse gene expression assays used the following probes: *Acta1* (Mm808218_g1), *Actn2* (Mm00473657_m1), *Bmp4* (Mm00432087_m1), *Cdx2* (Mm01212280_m1), *Col2a1* (Mm01309565_m1), *Eomes* (Mm01351985_m1), *Flk1* (Mm01222431 m1), *Gapdh* (Mm99999915_g1), *Gsc* (Mm00650681_g1), *Isl1* (Mm00517585_m1), *Lhx1* (Mm01297482_m1), *Meox1* (Mm00440285_m1), *Mesp1* (Mm00801883_g1), *Msgn1* (Mm00490407_s1), *Msx1* (Mm00440330_m1), *Myf5* (Mm00435125_m1), *Myh3* (Mm01332463_m1), *Myh6* (Mm00440354_m1), *Myh11* (Mm00443013_m1), *Myog* (Mm00446194_m1), *Nkx2.5* (Mm00657783_m1), *Nodal (*Mm00443040_m1), *Pax3* (Mm00435491_m1), *Pax6* (Mm00443081_m1), *Pax7* (Mm01354484_m1), *Pdgfr α* (Mm00440701_m1), *Pecam1* (Mm 01242584_m1), *Sox1* (Mm00486299_s1), *Sox2* (Mm03053810_s1), *Sox9* (Mm00448840_m1), *Sox17* (Mm00488363_m1), *T* (Mm00436877_m1), *Tbx6* (Mm01278677_m1), *Tcf15* (Mm00493442_m1), *Tnnt2* (Mm00441922_m1), and *Wnt3* (Mm00437336_m1). Human gene expression assays used the following probes: *Actn2* (Hs00153809_m1), *Bmp4* (Hs03676628_s1), *Cdh5* (Hs00901465_m1), *Cdx2* (Hs01078080_m1), *Cnn1* (Hs00154543_m1), *Eomes* (Hs00172872_m1), *Gapdh* (Hs02758991_g1), *Mesp1* (Hs00251489_m1), *Msx1* (Hs00427183_m1), *Myh11* (Hs00224610_m1), *Nodal* (Hs00415443_m1), *Nkx2.5* (Hs00231763_m1), *Pdgfr α* (Hs00998018_m1), Sox2 (Hs01053049_s1), *T* (Hs00610080_m1), *Tbx6* (Hs00365539_m1), *Tnnt2* (Hs00165960_m1) and *Wnt3a* (Hs00263977_m1). Expression of individual genes was subsequently analyzed by the Ct method, and was normalized to the expression of the housekeeping gene *Gapdh*.

Mouse ESC Differentiation

For mouse ESC differentiation, cells were suspended in modified serum-free differentiation (SFD) medium (Gadue et al., 2006). The SFD medium consisted of Iscove's modified Dulbecco's medium (Invitrogen, 12440-053) and Ham-F12 medium (Wako, 087-08335), supplemented with B27 (Invitrogen, 17504-044) and N2 supplements (Invitrogen, 17502-048), GlutaMAX, 10% bovine serum albumin (Invitrogen, P2489), L-ascorbic acid (Sigma-Aldrich, A4544), and 1-thioglycerol (Sigma-Aldrich, M6145) at a final concentration of 75,000 cells/mL in non-adherent Petri dishes, without any additional growth factors for 2 days. For cytokine-based directed cardiac

differentiation, EBs were dissociated, and the cells were reaggregated in the presence of recombinant human Activin A (R&D Systems, 338-AC), recombinant human BMP4 (R&D Systems, 314-BP), and recombinant human VEGF (R&D Systems, 293-VE) for 2 days. For transcription factor-based cardiac differentiation, Dox (Sigma-Aldrich, D9891, 1 μg/ml) was added to the SFD medium as indicated without exogenous factors. Inhibitors were used as indicated from day 0 to 3 of culture, and included dorsomorphin (Sigma-Aldrich, P5499), SB431542 (Wako, 192-16541), and IWR-1 (Sigma-Aldrich, I0161). For cardiomyocyte differentiation, cell clusters were dissociated and replated on gelatin-coated dishes in modified "cardiac conditions" (Kattman et al., 2006). In brief, 60,000 cells were cultured in 24-well flat-bottom plates in StemPro34 (Invitrogen, 10639-011) supplemented with L-ascorbic acid, recombinant human VEGF, recombinant human bFGF (R&D Systems, 233-FB), and recombinant human FGF10 (R&D Systems, 345-FG). For somite lineage differentiation, Dox was added to the SFD medium as indicated without exogenous factors. On day 5, cell clusters were dissociated and replated at 500,000 cells per well on a gelatin-coated six-well plate. Optimal pro-skeletal myogenic conditions and pro-chondrogenic conditions were SFD medium supplemented with 1 μM Y27632 (Wako, 253-00513) and 30 ng/mL GDF-5 (Prospec, cyt-941), respectively (Chan et al., 2016; Craft et al., 2013). For chimeric EB experiments, iTbx6 T-GFP ESCs and T-GFP ESCs were suspended in SFD media at an equivalent ratio and stimulated with Dox.

Generation of Tbx6 KO ESCs

We generated Tbx6 KO ESCs via homologous recombination with the CRISPR/Cas9 system. To generate CRISPR/Cas9 plasmids targeting the first exon of Tbx6, 20-bp target sequences were ligated into a pX330-U6-Chimeric_BB-CBh-hSpCas9 plasmid (Addgene, 42230) (Ran et al., 2013). A synthetic DNA fragment of homologous arms (500 bp each) with additional restriction enzyme sites (BglII and *Xho*I) in between the arms was introduced into the *Not*I and *Hind*III sites of pLSODN-3. An RFP-blasticidin resistance gene cassette was subsequently cloned between the homologous arms. The guide RNA (gRNA) sequences used to target Tbx6 and the synthetic DNA fragment are shown in Table S2. The CRISPR plasmid was co-transfected with the knock-in vector into mouse E14 ESCs. Three days after transfection, the ESCs were selected with blasticidin (2 μg/mL) treatment. Drug-resistant ESC clones were manually selected and expanded individually. Genomic DNA was isolated using the DNeasy blood and tissue kit (QIAGEN, 69504). Legitimate knock-in was determined by PCR and sequencing using the primers shown in Table S1. We obtained three clonal Tbx6 KO ESC lines (clones #1–3).

Lentiviral Infection and Generation of iTbx6 PSCs

The Dox-inducible lentiviral vector was generated by subcloning 3 × FLAG-mouse Tbx6 or human Tbx6 into the CSIV-TRE-RfA-UbC-KT lentiviral plasmid (RIKEN BSI) using the Gateway system (Invitrogen). The iTbx6 PSCs were generated using the modified lentiviral infection strategy, as previously reported (Kurita et al., 2013). In brief, we transfected the lentiviral vectors into 293T cells with pMDLg/pRRE and pCMV-VSV-G-RSV-Rev plasmids using Lipofectamine 2000 to generate lentiviruses (Invitrogen, 11668-019). Virus-containing media were collected after 48 h, and concentrated 10-fold by centrifugation before transduction. Mouse T-GFP ESCs or human iPSCs were transduced overnight with 4 μg/mL polybrene (Millipore, TR-1003-G) to generate iTbx6 T-GFP mESCs or iTbx6 hiPSCs, respectively. The infected PSCs expressed hKO, and the hKO^{+} homogeneous colonies were manually picked for clonal expansion. Dox was administered as indicated at 1 μg/mL for gene induction. To overexpress *Msx1* and *Cdx2* in the ESCs, we subcloned human cDNA into the CSII-CMV-RfA lentiviral vector (RIKEN BSI), generated lentiviruses, and infected iTbx6 T-GFP mESCs with the resulting lentiviruses.

Human PSC Differentiation

For cardiomyocyte differentiation, we cultured 100,000 cells hiPSCs with mTeSR1 (StemCell Technologies, ST-05850) in Matrigel (Corning, 356230) coated 12-well flat-bottom plates. The medium was changed to SP34 containing 5 ng/mL recombinant human ActivinA, 5 ng/mL recombinant human BMP4, and 5 ng/mL recombinant human bFGF on day 0. On day 2, the medium was changed to SP34. On day 3, the medium was changed to SP34 with 5 μM IWR-1 and 5 ng/mL recombinant human VEGF. Cells were maintained in recombinant human VEGF on day 7. For Dox-induced cardiac differentiation, Dox was added to the SP34 medium as indicated without exogenous factors.

Microarray Analyses

Genome-wide gene expression analyses were performed using the 3D-Gene Mouse Oligo Chip 25k (Toray Industries) as described previously (Muraoka et al., 2014; Yamakawa et al., 2015). RNA was extracted from EBs with or without Dox on days 2 and 4. The raw data for each spot were normalized by substitution with the mean intensity of the background signal determined by the combined signal intensities of all blank spots at 95% confidence intervals. Raw data intensities greater than 2 SDs of the background signal intensity were considered valid. Signals detected for each gene were normalized by the global normalization method. Hierarchical clustering, scatterplot analyses, and GO analyses were performed as described previously (Muraoka et al., 2014; Yamakawa et al., 2015).

Bioinformatics Analysis

The consensus sequence for the binding site of Tbx6 was identified from the JASPAR transcription factor binding database (http://jaspar.genereg.net/). The ECR browser (https://ecrbrowser.dcode.org) tool was used in the rVista genome browser (https://rvista.dcode.org) to identify the evolutionarily conserved DNA sequences in *Mesp1*, *Sox2*, and *Bmp4*, followed by T-box-binding site

prediction analysis. The rVista analysis of the ECR Browser alignment, spanning 40 kb including the *Mesp1*, *Sox2*, and *Bmp4* DNA region, was performed using transcription factor binding site (TFBS) matrices. A TFBS search with a 0.85 position weight (PMW) matrix cut-off identified highly conserved alignments.

Single-cell RNA-seq Analyses

Single-cell whole transcriptome in FACS sorted Flk1^{+} and CD41^{+} cells from E7.0–7.75 mouse embryos was analyzed using the public dataset (http://gastrulation.stemcells.cam.ac.uk/scialdone2016) (Scialdone et al., 2016).

Chromatin Immunoprecipitation (ChIP) Assays

ChIP analyses were performed as described previously (Lee et al., 2006). In brief, EBs were cross-linked with a 1% PFA solution for 15 min, quenched with 0.125 M glycine, and DNA was sonicated to obtain 300–500-bp DNA fragments through shearing using a Bioruptor, according to the manufacturer's protocol. Nuclear extracts were incubated with anti-Flag M2 antibody (Sigma-Aldrich, F3165), control IgG (Santa Cruz, sc-2025), anti-PolII antibody (Abcam, ab5408), and Dynabeads (Thermo Fisher Scientific, 10003D). qRT-PCR was performed using SYBR Green PCR Master Mix (Applied Biosystems, 4309155). Primers were designed as previously described (Costello et al., 2011), and the sequences of the primers are listed in Table S2.

QUANTIFICATION AND STATISTICAL ANALYSIS

Statistical Analyses

Differences between groups were examined for statistical significance using the Student's t tests or analysis of variance. Differences with *P value*s < 0.05 were regarded as significant.

DATA AND SOFTWARE AVAILABILITY

Data Resources

The accession number for the microarray data reported in this paper is NCBI GEO: GSE89820.